Chemical Engineering Science

Multi-objective optimization of heat exchanger network with disturbances based on graph theory and decoupling

--Manuscript Draft--

Manuscript Number:	CES-D-23-02734
Article Type:	Research paper
Section/Category:	Engineering Science
Keywords:	disturbance; decoupling; Excitation; graph theory; heat exchanger network; multi-objective optimization
Corresponding Author:	Guilian Liu Xi'an Jiaotong University Xi'an, CHINA
First Author:	Zixuan Zhang
Order of Authors:	Zixuan Zhang
	Liwen Zhao
	Ibrahim Tera
	Guilian Liu
Abstract:	The disturbance is a considerable challenge to the highly coupled chemical systems. This work aims to optimize the heat exchange network (HEN) from a decoupling perspective, considering the tradeoff between disturbance resistance and utility consumption. The HEN's directed graph is built based on the graph theory. Adjacency, Incidence, Reachability, and Laplacian matrices are employed to elucidate the HEN's topology structure and analyze the fluctuation transmission mechanism. The Excitation is defined to evaluate the HEN's decoupling degree. The superstructure-based multi-objective model is established for minimizing Excitation and energy consumption and solved by the combined improved Non-dominated Sorting Genetic Algorithm II (NSGA-II) and Depth-First Search algorithm. A coal-to-methanol process is studied using the proposed method. The identified utility consumption and Excitation are 29.6% and 264.50% less than the result of Aspen Energy Analyzer. The proposed method is efficient and can be used to design the HEN and evaluate the parameter fluctuations' impact.
Suggested Reviewers:	Dominic C. Y. Foo Dominic.Foo@nottingham.edu.my
	Petar Varbanov varbanov@fme.vutbr.cz
	Tim Walmsley tim.walmsley@waikato.ac.nz
	Haoshui Yu hayu@bio.aau.dk
	Jingzheng Ren jzhren@polyu.edu.hk
	Chang He hechang6@mail.sysu.edu.cn
Opposed Reviewers:	

Dear Editor,

This manuscript is submitted for publication in Chemical Engineering Science. Its title is " Multi-objective optimization of heat exchanger network with disturbances based on graph theory and decoupling". The corresponding author's name is Guilian Liu. The submitter's name is Guilian Liu also.

This manuscript aims to optimize the heat exchange network (HEN) from a decoupling perspective, considering the tradeoff between disturbance resistance and utility consumption. The HEN's directed graph is built based on the graph theory. Adjacency, Incidence, Reachability, and Laplacian matrices are employed to elucidate the HEN's topology structure and analyze the fluctuation transmission mechanism. The Excitation is defined to evaluate the HEN's decoupling degree. A superstructure-based multi-objective model is established for minimizing Excitation and energy consumption and solved by the combined improved Non-dominated Sorting Genetic Algorithm II (NSGA-II) and Depth-First Search algorithm. A coal-to-methanol process is studied using the proposed method. The identified utility consumption and Excitation are 29.6% and 264.50% less than the result of Aspen Energy Analyzer. The proposed method is efficient and can be used to design the HEN and evaluate the parameter fluctuations' impact.

The manuscript is essential for designing and operating chemical processes and has not been published before.

Best regards,

Guilian Liu
Department of Chemical Engineering
School of Chemical Engineering and Technology
Xi'an Jiaotong University
Xi'an 710049, P.R. China
Email: guilianliui@mail.xjtu.edu.cn

Research Highlights

- Directed graph and matrices are employed to elucidate the HEN’s topology structure
- The HEN’s decoupling degree and ability to resist disturbances is evaluated by the Excitation
- A superstructure-based model and improved NSGA-II are established for optimizing HEN
- The improved Utopian solution is targeted considering Excitation and energy consumption
- The utility consumption and Excitation are reduced by 29.6 % and 264.50 %

Multi-objective optimization of heat exchanger network with disturbances based on graph theory and decoupling

Zixuan Zhang[1], Liwen Zhao[1], Ibrahim Tera[1], Guilian Liu[1,2]*

1. School of Chemical Engineering and Technology, Xi'an Jiaotong University, Xi'an, Shaanxi, 710049, China
2. Engineering Research Center of New Energy System Engineering and Equipment, University of Shaanxi Province, Xi'an, Shaanxi, 710049, China

Abstract: The disturbance is a considerable challenge to the highly coupled chemical systems. This work aims to optimize the heat exchange network (HEN) from a decoupling perspective, considering the tradeoff between disturbance resistance and utility consumption. The HEN's directed graph is built based on the graph theory. Adjacency, Incidence, Reachability, and Laplacian matrices are employed to elucidate the HEN's topology structure and analyze the fluctuation transmission mechanism. The Excitation is defined to evaluate the HEN's decoupling degree. The superstructure-based multi-objective model is established for minimizing Excitation and energy consumption and solved by the combined improved Non-dominated Sorting Genetic Algorithm II (NSGA-II) and Depth-First

*Corresponding author: Prof. Guilian Liu, E-mail: guilianliui@mail.xjtu.edu.cn.

Search algorithm. A coal-to-methanol process is studied using the proposed method. The identified utility consumption and Excitation are 29.6% and 264.50% less than the result of Aspen Energy Analyzer. The proposed method is efficient and can be used to design the HEN and evaluate the parameter fluctuations' impact.

Keywords: disturbance; decoupling; Excitation; graph theory; heat exchanger network; multi-objective optimization

1. Introduction

The chemical industry represents one of the key sectors of the national economy. It consumes a large amount of resources and generates a variety of pollutants. More than 50% of the chemical industry's direct emissions come from the combustion of fossil fuels. Today, the industry faces two challenges, namely the continued development of the sector and the reduction of carbon emissions. To achieve carbon neutrality, it is crucial to significantly reduce or eliminate fossil fuels from raw materials. Chemical companies need to keep energy and raw material consumption to a minimum level and maximize the device's operational efficiency and production flexibility.

The chemical production process comprises reactors, separators, heat exchanger networks (HENs), and utilities. The reactors and separators influence the HEN, as their feeds and products are generally the hot and cold streams of HEN. Disturbances of reactors and separators, such as catalyst deactivation, equipment failure, human-made faults, and extreme weather, induce the HEN's uncertainties,

affecting the optimal match between hot and cold streams. The causes of disturbances and their influence on the system are shown in Fig. 1. The disturbance and uncertainty affect the optimal match between hot and cold streams, the HEN's minimum utility consumption, and the production's safety and stability. Hence, optimizing HEN with uncertain parameters should be given more attention.

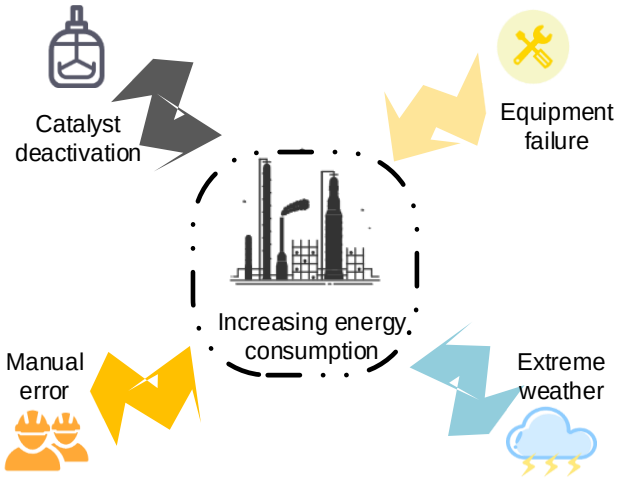

Fig. 1 Factors causing the disturbances of chemical processes

Since the 1980s, scholars have developed multiple thermodynamic and mathematical programming methods to design and optimize HEN. The pinch technology is the most influential among them and has been widely used to synthesize HEN (Linnhoff and Hindmarsh, 1983). The mathematical programming methods can automatically target a HEN with the minimum annualized cost, no matter the problem's complexity. Some of these mathematical programming methods are widely used, including the mixed integer linear programming (MILP) methods based on the transshipment model (Papoulias and Grossmann, 1983),

the mixed integer nonlinear programming (MINLP) transshipment model proposed by Floudas et al. (1986), and the superstructure model (Yee et al., 1990).

Scholars analyzed the impact of uncertain parameters on utility consumption, considering different units and their coupling with HEN. Hafizan et al. (2019) established a mathematical model for minimizing costs, with the supply temperature fluctuations, heat exchanger size, bypass location, and economic performance considered. Ryu et al. (2020) proposed a generalized framework for formulating superstructure-based optimization models for holistic process synthesis. Zhang et al. (2020) combined the pinch and mathematical programming methods and proposed an integration approach for the reactor-distillation column-recycle-HEN system, which can determine the minimum energy consumption and corresponding reactor as well as distillation parameters efficiently. Mohanan and Jogwar (2022) utilized a new energy allocation method to control the transmission path of disturbances, thereby reducing the impact of disturbances on utility consumption. Zhao and Liu (2023) developed bottleneck identification and debottlenecking strategies based on topology analysis for HEN with disturbances. However, the coupling between different units significantly increases the model's complexity, raising the computational cost and bringing challenges to the process system's stable production.

Multiple sensitivity analysis models were developed to study the influence of fluctuations on the HENs and are suitable for both linear and nonlinear parameter relations. The sensitivity method developed based on HEN's inherent linear characteristics (Ratnam and Patwardhan, 1991) has high calculation efficiency and

can be applied to cases with multiple and significant parameter variations. Jiang et al. (2014) evaluated the HEN's flexibility and retrofitted the HEN by strengthening the most sensitive heat exchanger and avoiding the addition of new equipment. Li et al. (2015) constructed a direction matrix to describe the deviation of uncertain parameters and proposed a subnetting decoupling strategy for large-scale and non-convex problems. The proposed method is proven to be efficient. Sensitivity analysis has been widely used in operation units but is rarely carried out in designing HENs with resistance to fluctuations. Cardoso-Fernández et al. (2023) proposed a method with an artificial intelligence model for global sensitivity analysis of a generator-absorber heat exchange system's thermal performance with a hybrid energy source.

A flexible HEN can resist the influence of parameter fluctuations. Aguilera and Nasini (1995) conducted flexible testing for HEN with the heat capacity flow rate change. Considering the flexible HEN's structure and area, Li et al. (2014) developed a step-by-step optimization method to minimize the total annualized cost and heat exchange area; the direction matrix is used to optimize the operational flexibility and critical operating points of HEN. Miranda et al. (2016) established a superstructure model for minimizing the total annualized cost of the multi-period HEN, and the excessive heat exchange area was avoided by unfixing the matching of each device in different periods. Kang and Liu (2018a) developed a three-step optimization strategy for multi-period flexible HENs, including synthesizing multi-period HENs, flexible analysis, and sub-period bottlenecking. In addition, the application of the proposed method is illustrated by a HEN of a

vacuum wax oil hydrogenation unit (Kang and Liu, 2018b). Based on fuzzy game theory, Tian and Li (2023) determined the contribution of each plant when the decision-making environment is uncertain and optimized the inter-plant HEN under uncertain flow.

In the references introduced above, the influence of parameter fluctuations has been analyzed regarding the sensitivity and operational flexibility of HEN, while the impact of HEN's topology on parameter fluctuations was not investigated. Meanwhile, no suitable optimization strategy is provided for situations where parameter fluctuations exceed the HEN's tolerance.

Based on the complex HEN's topology, a method was developed to constrain the size of the feasible region and successfully solve the problem of "combination explosion" (Wang et al., 1999); the genetic algorithm was used to solve the corresponding model. Zhu et al. (1996) proposed a method to identify load loops and downstream paths based on spanning trees. Combining the thermodynamic method and graph theory, Gu and Vassiliadis (2014) demonstrated that Euler's formula cannot always be applied to pinch technology. Kang et al. (2016) reconstructed the hierarchical clustering in the context of graph theory, optimized the structural coupling between control and operational variables, and successfully applied it to synthesizing fuel cell systems and HENs. Although the above studies have combined the graph theory into the HEN optimization, no research employs the graph theory to analyze the influence of parameter fluctuations.

For different models considering uncertain parameters, especially multi-objective optimization models, selecting the appropriate algorithm is also one of the key

steps toward obtaining a good solution. Ye et al. (2014) used robust optimization and two-stage stochastic programming to solve the problem of large steel mills' continuous casting with uncertain demand. Li et al. (2016) established a data-driven distillation model for highly integrated refining and chemical enterprises and a global optimization framework to predict product yield and performance. Zeng et al. (2018) established a multi-stage MILP model to minimize the operating cost of steel plants with by-product gas, steam, and electricity. Aguitoni et al. (2018) divided the HEN synthesis problem into inner and outer layers and used a genetic algorithm combined with a differential evolution algorithm to solve it. A food-energy-water nexus model framework was established (Nie et al., 2018), and a two-stage decomposition strategy was used to solve multi-scale and multi-stage planning and scheduling problems (Nie et al., 2019). The random walk and forced evolutionary algorithms were combined to solve a multi-objective optimization problem using a non-structural model (Xu and Cui, 2023). With minimizing energy cost and CO_2 emission taken as objectives, the proposed method was applied to optimize the HEN of a crude oil distillation unit (Xu et al., 2023). Huang et al. (2023) established a multi-objective optimization model for the power-heat exchange coupling network and solved it with the ε-constraint method. However, no model and algorithm could describe the strength of the HEN's resistance to parameter fluctuations from the decoupling perspective.

According to an open literature survey, most studies on the synthesis of HEN with disturbances focus on the trade-off between the HEN's operational flexibility and annual total cost, while the mechanism of fluctuation transmission and its impact

remains unclear; the topology structure of the HEN was not studied from the decoupling perspective, which can minimize the heat, mass, and momentum transfer between units through reducing the fluctuation transmission in the system. Besides, the decoupling is not always a win-win situation; it also increases utility consumption. Enhancing HEN flexibility will increase investment costs for a more significant heat transfer area margin. While the proposed methods could not determine the HEN's resistance to parameter fluctuations when exceeding the operating margin.

A HEN can be viewed as a graph, with streams as edges and heat exchangers as nodes; the transmission of parameter fluctuations in HEN described in graph theory can significantly facilitate the computation from a decoupling perspective. This study aims to establish an evaluation model to analyze the impact of parameter fluctuations on HEN with graph theory and a multi-objective optimization model to minimize the utility consumption and decoupling degree (Excitation) and solve it with the improved Non-dominated Sorting Genetic Algorithm II (NSGA-II). A methanol synthesis system will be studied to demonstrate the rationality of the model.

2. Problem description and challenges

In chemical production, various factors, such as catalyst activity, extreme weather, equipment failures, and manual operations, can lead to uncertain parameters. To ensure the system's stable operation under uncertain parameters, engineers usually leave a certain design margin for the operating unit, while increasing the

margin increases investment costs. Generally, it is necessary to design the devices with suitable margins while improving the system's adaptability to uncertain factors through other measures.

Units or devices affect each other. For example, in Fig. 2 (a), the reactor's outlet stream is used in the distillation column's reboiler to provide energy, and the two devices are coupled. In Fig. 2 (b), the reactor's outlet stream and the distillation column's reboiler are cooled and heated by utilities, and the reactor and distillation column are decoupled. When the temperature of the reactor's outlet stream changes due to factors such as catalyst deactivation, the performance of the distillation column shown in Fig. 2 (a) will be affected, while the distillation column shown in Fig. 2 (b) is not affected. Hence, decoupling the devices can reduce the influence of uncertain parameters. However, the energy consumption and operating cost will increase. Decoupling the units or devices and targeting the suitable fewer devices to enhance instead of all is crucial. Thus, the investment costs can be reduced, and the system's ability to resist fluctuations is enhanced.

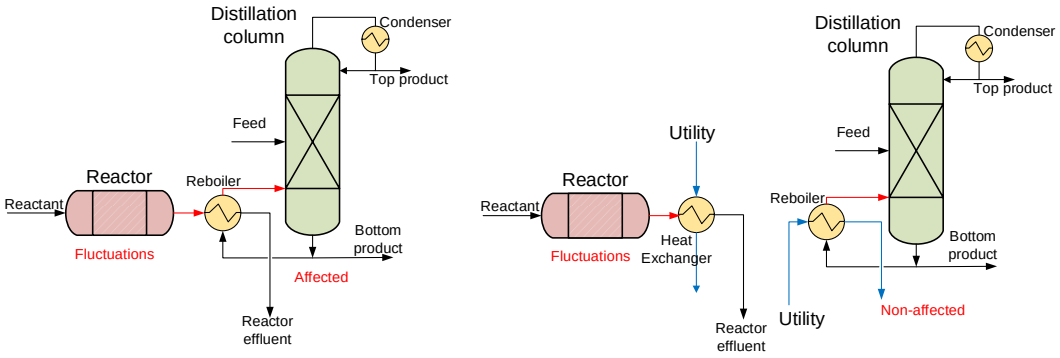

(a) Coupled reactor and distillation column; (b) Decoupled reactor and distillation column

Fig. 2 Coupling and decoupling relationship between units

The hot and cold streams in the HEN couple through the heat exchanger. Excessive or unreasonable coupling will increase the system's complexity and have a negative effect on the system's stability. It is necessary to decouple the HEN to enhance the ability to resist fluctuations. On the other hand, decoupling the HEN will increase utility consumption. The contradictory relationship between the coupling and decoupling of heat exchangers is shown in Fig. 3.

There are two main challenges in designing a HEN with low utility costs and resistance to parameter fluctuations. One is to develop a reasonable model to measure the decoupling degree of units; the other is to design a multi-objective optimization algorithm to trade off coupling and decoupling and enhance the HEN's ability to resist parameter fluctuations with less utility increment.

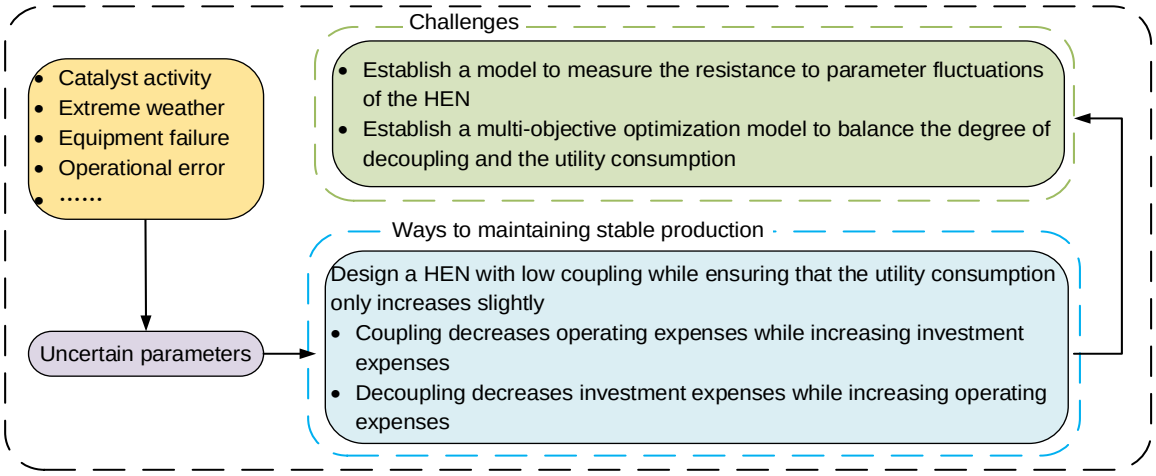

Fig. 3 Contradictory relationship between coupling and decoupling of units

This study aims to figure out how to design a HEN with low coupling while ensuring that the utility consumption increases slightly and establish an improved superstructure model with the energy consumption and the disturbance resistance

considered. The Excitation, defined as the fluctuation degree of the whole network excited by the parameter changes, is put forward to measure the decoupling between units, i.e., the ability to resist fluctuations. Since the parameter fluctuation is related to the topological structure between units, the graph theory will be applied to transform the HEN into directed graph (Digraph) and improve the NSGA-II with decapitation disaster, population migration, and gene pool strategies. Forbidden matching and maximum energy matching strategies will be introduced to transform the constraints and improve the quality of the initial solution. The effectiveness and feasibility of the model will be verified through comparison and analysis.

3. Directed graph (Digraph) of HEN

3.1 Transformation of HEN to Digraph

The grid diagram shown in Fig. 4 is widely employed to illustrate the HENs. A vertical line joining two heat exchangers (denoted by E) on the two streams represents a heat exchange match. HE indicates the heater consuming heating utility, while CE stands for the cooler using the cooling utility. This diagram can clearly distinguish whether there is a heat exchange between streams and the order of heat exchange, while it cannot show a HEN's actual topology nor be used in automatic computing.

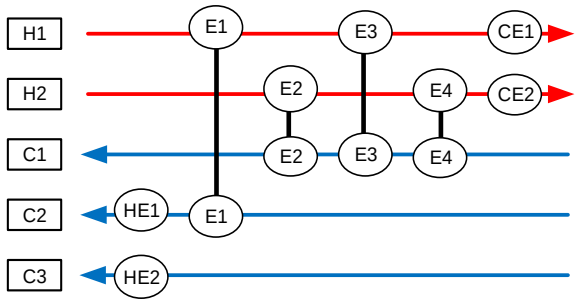

Fig. 4 The grid diagram of a five-stream HEN

The Digraph can reflect the topological relationship between the heat exchanger and the stream. The relationship between the HEN's geometric and physical meanings can be established by employing algebraic graph theory, which benefits the storage and solution of the HEN's structure. Based on this, the influence of parameter fluctuation on the HEN can be analyzed. The HEN's grid diagram can be transferred into a Digraph according to the following rules:

1) The initial and target of each stream are taken as virtual nodes, and each virtual node's in-degree or out-degree is only allowed to be 1. The in-degree is the number of directed lines that inlet the node; the out-degree is the number of directed lines leaving the node;

2) Each heat exchanger is taken as a real node; for the real node corresponding utility heat exchanger, both its in-degree and out-degree are 1; for a real node corresponding to the heat exchanger between two streams, both its in-degree and out-degree are 2;

3) If a stream flows between two nodes, a directed line is added according to the stream's flow direction.

Based on these rules, the HEN shown in Fig. 4 can be transformed into a Digraph shown in Fig. 5.

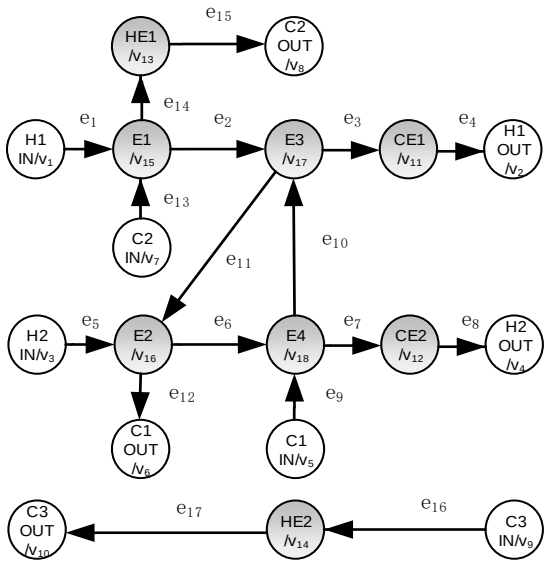

Fig. 5 Digraph of the HEN shown in Fig. 4

3.2 Adjacency and incidence matrices of HEN

The HEN's Digraph can be expressed by the matrix, which is effective and necessary for analyzing the parameter fluctuation with the computer. The adjacency and incidence matrices, suitable for different analysis scenarios, will be employed to represent the HEN in this work.

Adjacency matrix

Set graph $G = <V,E>$, with a node set $V = \{v_1, v_2, ..., v_n\}$ and an edge set $E = \{e_1, e_2, ..., e_m\}$. The adjacency matrix is a $n \times n$ matrix, whose element can be identified according to Eq. (1) (Deo, 1975).

$$Adjacency_{ij} = \begin{cases} 0 & \text{There is no edge from } v_i \text{ to } v_j \text{ in } E. \\ 1 & \text{There is an edge/edges from } v_i \text{ to } v_j \text{ in } E. \end{cases} \quad (1)$$

For the HEN shown in Fig. 5, the serial numbers of nodes are shown in Table A. 1 in Appendix A; the correspondence between edges and stream is shown in Table A. 2. There is a stream flow from heat exchanger E1 to E3, which means there is a directed edge from node v_{15} to node v_{17}, $Adjacency_{15,17} = 1$. On the contrary, no stream flows directly from E1 to E2, which means there is no directed edge from node v_{15} to node v_{16}, $Adjacency_{15,16} = 0$. The adjacency matrix of the Digraph shown in Fig. 5 is illustrated in Eq.(2).

$$Adjacency = \begin{array}{c} \\ v_1 \\ v_2 \\ v_3 \\ v_4 \\ v_5 \\ v_6 \\ v_7 \\ v_8 \\ v_9 \\ v_{10} \\ v_{11} \\ v_{12} \\ v_{13} \\ v_{14} \\ v_{15} \\ v_{16} \\ v_{17} \\ v_{18} \end{array} \begin{array}{c} \begin{array}{cccccccccccccccccc} v_1 & v_2 & v_3 & v_4 & v_5 & v_6 & v_7 & v_8 & v_9 & v_{10} & v_{11} & v_{12} & v_{13} & v_{14} & v_{15} & v_{16} & v_{17} & v_{18} \end{array} \\ \begin{bmatrix} 0 & 0 & 0 & 0 & 0 & 0 & 0 & 0 & 0 & 0 & 0 & 0 & 0 & 0 & 1 & 0 & 0 & 0 \\ 0 & 0 & 0 & 0 & 0 & 0 & 0 & 0 & 0 & 0 & 0 & 0 & 0 & 0 & 0 & 0 & 0 & 0 \\ 0 & 0 & 0 & 0 & 0 & 0 & 0 & 0 & 0 & 0 & 0 & 0 & 0 & 0 & 0 & 1 & 0 & 0 \\ 0 & 0 & 0 & 0 & 0 & 0 & 0 & 0 & 0 & 0 & 0 & 0 & 0 & 0 & 0 & 0 & 0 & 0 \\ 0 & 0 & 0 & 0 & 0 & 0 & 0 & 0 & 0 & 0 & 0 & 0 & 0 & 0 & 0 & 0 & 0 & 1 \\ 0 & 0 & 0 & 0 & 0 & 0 & 0 & 0 & 0 & 0 & 0 & 0 & 0 & 0 & 0 & 0 & 0 & 0 \\ 0 & 0 & 0 & 0 & 0 & 0 & 0 & 0 & 0 & 0 & 0 & 0 & 0 & 0 & 1 & 0 & 0 & 0 \\ 0 & 0 & 0 & 0 & 0 & 0 & 0 & 0 & 0 & 0 & 0 & 0 & 0 & 0 & 0 & 0 & 0 & 0 \\ 0 & 0 & 0 & 0 & 0 & 0 & 0 & 0 & 0 & 0 & 0 & 0 & 0 & 1 & 0 & 0 & 0 & 0 \\ 0 & 0 & 0 & 0 & 0 & 0 & 0 & 0 & 0 & 0 & 0 & 0 & 0 & 0 & 0 & 0 & 0 & 0 \\ 0 & 1 & 0 & 0 & 0 & 0 & 0 & 0 & 0 & 0 & 0 & 0 & 0 & 0 & 0 & 0 & 0 & 0 \\ 0 & 0 & 0 & 1 & 0 & 0 & 0 & 0 & 0 & 0 & 0 & 0 & 0 & 0 & 0 & 0 & 0 & 0 \\ 0 & 0 & 0 & 0 & 0 & 0 & 0 & 1 & 0 & 0 & 0 & 0 & 0 & 0 & 0 & 0 & 0 & 0 \\ 0 & 0 & 0 & 0 & 0 & 0 & 0 & 0 & 0 & 1 & 0 & 0 & 0 & 0 & 0 & 0 & 0 & 0 \\ 0 & 0 & 0 & 0 & 0 & 0 & 0 & 0 & 0 & 0 & 0 & 0 & 1 & 0 & 0 & 0 & 1 & 0 \\ 0 & 0 & 0 & 0 & 0 & 1 & 0 & 0 & 0 & 0 & 0 & 0 & 0 & 0 & 0 & 0 & 0 & 1 \\ 0 & 0 & 0 & 0 & 0 & 0 & 0 & 0 & 0 & 0 & 1 & 0 & 0 & 0 & 0 & 1 & 0 & 0 \\ 0 & 0 & 0 & 0 & 0 & 0 & 0 & 0 & 0 & 0 & 0 & 1 & 0 & 0 & 0 & 0 & 1 & 0 \end{bmatrix} \end{array} \quad (2)$$

In the adjacency matrix, the out-degree of node v_i ($d_j^{(+)}$) equals $\sum_{i=0}^{n} Adjacency_{ij}$, and the in-degree of node v_j ($d_j^{(-)}$) is $\sum_{j=0}^{n} Adjacency_{ij}$. The adjacency matrix stores the topological relationship between the heat exchangers and can be used to analyze the transfer of fluctuations among heat exchangers.

Incidence matrix

A graph *G*'s incidence matrix is a $n \times m$ matrix, where *n* is the number of nodes and *m* is the number of edges. Its element is defined by Eq. (3) (Deo, 1975).

$$Incidence_{ij} = \begin{cases} -1 & \text{Node } v_i \text{ is the source of the directed edge } e_j. \\ 1 & \text{Node } v_i \text{ is a sink of a directed edge } e_j. \\ 0 & \text{Others.} \end{cases} \quad (3)$$

In the incidence matrix, the in-degree minus out-degree of node v_i ($d_i^{(-)} - d_i^{(+)}$) is $\sum_{j=0}^{m} Incidence_{ij}$, which equals 0. The incidence matrix stores the connection information between edges and nodes, provides the physical information of the inlet and outlet streams of the heat exchanger, and also reveals the topological position of the streams that cause the fluctuation of the HEN. In the Digraph shown in Fig. 5, a stream flows directly from E1 to E3 and does not flow through E2, that is, the source of edge e_2 is node v_{15}, the sink is node v_{17}, and the node v_{16} is not related, then $Incidence_{2,15} = -1$, $Incidence_{2,17} = 1$, and $Incidence_{2,16} = 0$. The incidence matrix of this Digraph is shown in Eq. (4).

$$
Incidence = \begin{array}{c} \\ v_1 \\ v_2 \\ v_3 \\ v_4 \\ v_5 \\ v_6 \\ v_7 \\ v_8 \\ v_9 \\ v_{10} \\ v_{11} \\ v_{12} \\ v_{13} \\ v_{14} \\ v_{15} \\ v_{16} \\ v_{17} \\ v_{18} \end{array}
\begin{array}{c}
\begin{array}{ccccccccccccccccc} e_1 & e_2 & e_3 & e_4 & e_5 & e_6 & e_7 & e_8 & e_9 & e_{10} & e_{11} & e_{12} & e_{13} & e_{14} & e_{15} & e_{16} & e_{17} \end{array} \\
\begin{bmatrix}
-1 & 0 & 0 & 0 & 0 & 0 & 0 & 0 & 0 & 0 & 0 & 0 & 0 & 0 & 0 & 0 & 0 \\
0 & 0 & 0 & 1 & 0 & 0 & 0 & 0 & 0 & 0 & 0 & 0 & 0 & 0 & 0 & 0 & 0 \\
0 & 0 & 0 & 0 & -1 & 0 & 0 & 0 & 0 & 0 & 0 & 0 & 0 & 0 & 0 & 0 & 0 \\
0 & 0 & 0 & 0 & 0 & 0 & 0 & 1 & 0 & 0 & 0 & 0 & 0 & 0 & 0 & 0 & 0 \\
0 & 0 & 0 & 0 & 0 & 0 & 0 & 0 & -1 & 0 & 0 & 0 & 0 & 0 & 0 & 0 & 0 \\
0 & 0 & 0 & 0 & 0 & 0 & 0 & 0 & 0 & 0 & 0 & 1 & 0 & 0 & 0 & 0 & 0 \\
0 & 0 & 0 & 0 & 0 & 0 & 0 & 0 & 0 & 0 & 0 & 0 & -1 & 0 & 0 & 0 & 0 \\
0 & 0 & 0 & 0 & 0 & 0 & 0 & 0 & 0 & 0 & 0 & 0 & 0 & 0 & 1 & 0 & 0 \\
0 & 0 & 0 & 0 & 0 & 0 & 0 & 0 & 0 & 0 & 0 & 0 & 0 & 0 & 0 & -1 & 0 \\
0 & 0 & 0 & 0 & 0 & 0 & 0 & 0 & 0 & 0 & 0 & 0 & 0 & 0 & 0 & 0 & 1 \\
0 & 0 & 1 & -1 & 0 & 0 & 0 & 0 & 0 & 0 & 0 & 0 & 0 & 0 & 0 & 0 & 0 \\
0 & 0 & 0 & 0 & 0 & 0 & 1 & -1 & 0 & 0 & 0 & 0 & 0 & 0 & 0 & 0 & 0 \\
0 & 0 & 0 & 0 & 0 & 0 & 0 & 0 & 0 & 0 & 0 & 0 & 0 & 1 & -1 & 0 & 0 \\
0 & 0 & 0 & 0 & 0 & 0 & 0 & 0 & 0 & 0 & 0 & 0 & 0 & 0 & 0 & 1 & -1 \\
1 & -1 & 0 & 0 & 0 & 0 & 0 & 0 & 0 & 0 & 0 & 0 & 1 & -1 & 0 & 0 & 0 \\
0 & 0 & 0 & 0 & 1 & -1 & 0 & 0 & 0 & 0 & 1 & -1 & 0 & 0 & 0 & 0 & 0 \\
0 & 1 & -1 & 0 & 0 & 0 & 0 & 0 & 0 & 1 & -1 & 0 & 0 & 0 & 0 & 0 & 0 \\
0 & 0 & 0 & 0 & 0 & 1 & -1 & 0 & 1 & -1 & 0 & 0 & 0 & 0 & 0 & 0 & 0
\end{bmatrix}
\end{array}
\tag{4}
$$

3.3 Reachability of parameter fluctuations

Parameter fluctuations can be directly or indirectly transmitted downstream through the heat exchanger. It is essential to explore how a stream's fluctuation can be transmitted downstream and affect the heat exchangers' load. The HEN's structure is usually quite complex, and it is impossible to observe whether there is a path between two nodes. The reachable matrix is introduced to determine whether the parameter fluctuation of a stream will be transmitted downstream. Graph *G*'s reachable matrix is a $n \times n$ matrix. For any $\{v_i, v_j\} \in V$, if there is a path connecting v_i and v_j, these two nodes are reachable, and the parameter fluctuation can be transmitted from v_i to v_j. The element of the reachable matrix is defined in Eq.(5).

$$Reachability_{ij} = \begin{cases} 0 & \text{There is no pathway from } v_i \text{ to } v_j. \\ 1 & \text{There is a pathway from } v_i \text{ to } v_j. \end{cases} \quad (5)$$

The reachable matrix can be determined based on the adjacency matrix and the multiplication, power multiplication, Warshall algorithm (Warshall, 1962), or Tarjan algorithm (Tarjan, 1971). The pseudo-code of targeting the reachable matrix by the multiplication algorithm is shown in

Table A. 3. The reachability matrix of Fig. 5 is shown in Eq. (6).

$$Reachability = \begin{array}{c} \\ v_1 \\ v_2 \\ v_3 \\ v_4 \\ v_5 \\ v_6 \\ v_7 \\ v_8 \\ v_9 \\ v_{10} \\ v_{11} \\ v_{12} \\ v_{13} \\ v_{14} \\ v_{15} \\ v_{16} \\ v_{17} \\ v_{18} \end{array} \begin{array}{c} \begin{array}{cccccccccccccccccc} v_1 & v_2 & v_3 & v_4 & v_5 & v_6 & v_7 & v_8 & v_9 & v_{10} & v_{11} & v_{12} & v_{13} & v_{14} & v_{15} & v_{16} & v_{17} & v_{18} \end{array} \\ \begin{bmatrix} 0 & 1 & 0 & 1 & 0 & 1 & 0 & 1 & 0 & 0 & 1 & 1 & 1 & 0 & 1 & 1 & 1 & 1 \\ 0 & 0 & 0 & 0 & 0 & 0 & 0 & 0 & 0 & 0 & 0 & 0 & 0 & 0 & 0 & 0 & 0 & 0 \\ 0 & 1 & 0 & 1 & 0 & 1 & 0 & 0 & 0 & 0 & 1 & 1 & 0 & 0 & 0 & 1 & 1 & 1 \\ 0 & 0 & 0 & 0 & 0 & 0 & 0 & 0 & 0 & 0 & 0 & 0 & 0 & 0 & 0 & 0 & 0 & 0 \\ 0 & 1 & 0 & 1 & 0 & 1 & 0 & 0 & 0 & 0 & 1 & 1 & 0 & 0 & 0 & 1 & 1 & 1 \\ 0 & 0 & 0 & 0 & 0 & 0 & 0 & 0 & 0 & 0 & 0 & 0 & 0 & 0 & 0 & 0 & 0 & 0 \\ 0 & 1 & 0 & 1 & 0 & 1 & 0 & 1 & 0 & 0 & 1 & 1 & 1 & 0 & 1 & 1 & 1 & 1 \\ 0 & 0 & 0 & 0 & 0 & 0 & 0 & 0 & 0 & 0 & 0 & 0 & 0 & 0 & 0 & 0 & 0 & 0 \\ 0 & 0 & 0 & 0 & 0 & 0 & 0 & 0 & 0 & 1 & 0 & 0 & 0 & 1 & 0 & 0 & 0 & 0 \\ 0 & 0 & 0 & 0 & 0 & 0 & 0 & 0 & 0 & 0 & 0 & 0 & 0 & 0 & 0 & 0 & 0 & 0 \\ 0 & 1 & 0 & 0 & 0 & 0 & 0 & 0 & 0 & 0 & 0 & 0 & 0 & 0 & 0 & 0 & 0 & 0 \\ 0 & 0 & 0 & 1 & 0 & 0 & 0 & 0 & 0 & 0 & 0 & 0 & 0 & 0 & 0 & 0 & 0 & 0 \\ 0 & 0 & 0 & 0 & 0 & 0 & 0 & 1 & 0 & 0 & 0 & 0 & 0 & 0 & 0 & 0 & 0 & 0 \\ 0 & 0 & 0 & 0 & 0 & 0 & 0 & 0 & 0 & 1 & 0 & 0 & 0 & 0 & 0 & 0 & 0 & 0 \\ 0 & 1 & 0 & 1 & 0 & 1 & 0 & 1 & 0 & 0 & 1 & 1 & 1 & 0 & 0 & 1 & 1 & 1 \\ 0 & 1 & 0 & 0 & 0 & 1 & 0 & 0 & 0 & 0 & 1 & 1 & 0 & 0 & 0 & 0 & 1 & 1 \\ 0 & 1 & 0 & 1 & 0 & 1 & 0 & 0 & 0 & 0 & 1 & 1 & 0 & 0 & 0 & 1 & 0 & 1 \\ 0 & 1 & 0 & 1 & 0 & 1 & 0 & 0 & 0 & 0 & 1 & 1 & 0 & 0 & 0 & 1 & 1 & 0 \end{bmatrix} \end{array} \quad (6)$$

3.4 Irrelevant subsystem

Irrelevant subsystems are subsystems that are not connected in any way. For a HEN, two subsystems without heat or mass transfer are independent. And parameter variations between irrelevant subsystems cannot be transmitted to each other.

Graph theory defines the connected component as a maximal connected subgraph. Any two nodes in a connected component are reachable in at least one direction, and there are no shared nodes and edges between different connected components. In the Digraph of the HEN, the edge represents the mass transfer, and the node represents the heat transfer. The connected components without heat and mass exchange can be taken as irrelevant subsystems. For a HEN with a certain number of heat exchangers, the more the irrelevant subsystems, the lower complexity of the whole system, the higher the degree of decoupling, and the less influence the parameter fluctuations.

The degree matrix and Laplace matrix are introduced to identify the HEN's irrelevant subsystems. Since these two matrices are only applicable to undirected graphs and the transformation of a Digraph into an undirected graph does not affect its irrelevant subsystems, the adjacency matrix is first transformed into the adjacency matrix of the undirected graph ($Adjacency'$), as shown by Eq. (7).

$$Adjacency' = Adjacency \vee Adjacency^{\top} \tag{7}$$

Where $\vee$ is the symbol of OR operation and the $Adjacency^{\top}$ is the transpose matrix of the $Adjacency$.

For graph *G*, the degree matrix is a $n \times n$ diagonal matrix; each diagonal element can be calculated according to Eq.(8). The Laplacian matrix is a $n \times n$ matrix and can be calculated based on the degree matrix and the adjacency matrix of the undirected graph, as shown by Eq. (9). The sum of each row and column of the Laplacian matrix is 0. For the system shown in Fig. 5, the degree matrix is shown in Eq. (10), and the Laplacian matrix is shown in Eq. (11).

$$Degree_{ii} = \sum_{j=0}^{n} Adjacency'_{ij} \tag{8}$$

$$Laplacian = Degree - Adjacency' \tag{9}$$

$$Degree = \begin{array}{c} \\ v_1 \\ v_2 \\ v_3 \\ v_4 \\ v_5 \\ v_6 \\ v_7 \\ v_8 \\ v_9 \\ v_{10} \\ v_{11} \\ v_{12} \\ v_{13} \\ v_{14} \\ v_{15} \\ v_{16} \\ v_{17} \\ v_{18} \end{array} \begin{array}{c} \begin{array}{cccccccccccccccccc} v_1 & v_2 & v_3 & v_4 & v_5 & v_6 & v_7 & v_8 & v_9 & v_{10} & v_{11} & v_{12} & v_{13} & v_{14} & v_{15} & v_{16} & v_{17} & v_{18} \end{array} \\ \begin{bmatrix} 1 & 0 & 0 & 0 & 0 & 0 & 0 & 0 & 0 & 0 & 0 & 0 & 0 & 0 & 0 & 0 & 0 & 0 \\ 0 & 1 & 0 & 0 & 0 & 0 & 0 & 0 & 0 & 0 & 0 & 0 & 0 & 0 & 0 & 0 & 0 & 0 \\ 0 & 0 & 1 & 0 & 0 & 0 & 0 & 0 & 0 & 0 & 0 & 0 & 0 & 0 & 0 & 0 & 0 & 0 \\ 0 & 0 & 0 & 1 & 0 & 0 & 0 & 0 & 0 & 0 & 0 & 0 & 0 & 0 & 0 & 0 & 0 & 0 \\ 0 & 0 & 0 & 0 & 1 & 0 & 0 & 0 & 0 & 0 & 0 & 0 & 0 & 0 & 0 & 0 & 0 & 0 \\ 0 & 0 & 0 & 0 & 0 & 1 & 0 & 0 & 0 & 0 & 0 & 0 & 0 & 0 & 0 & 0 & 0 & 0 \\ 0 & 0 & 0 & 0 & 0 & 0 & 1 & 0 & 0 & 0 & 0 & 0 & 0 & 0 & 0 & 0 & 0 & 0 \\ 0 & 0 & 0 & 0 & 0 & 0 & 0 & 1 & 0 & 0 & 0 & 0 & 0 & 0 & 0 & 0 & 0 & 0 \\ 0 & 0 & 0 & 0 & 0 & 0 & 0 & 0 & 1 & 0 & 0 & 0 & 0 & 0 & 0 & 0 & 0 & 0 \\ 0 & 0 & 0 & 0 & 0 & 0 & 0 & 0 & 0 & 1 & 0 & 0 & 0 & 0 & 0 & 0 & 0 & 0 \\ 0 & 0 & 0 & 0 & 0 & 0 & 0 & 0 & 0 & 0 & 2 & 0 & 0 & 0 & 0 & 0 & 0 & 0 \\ 0 & 0 & 0 & 0 & 0 & 0 & 0 & 0 & 0 & 0 & 0 & 2 & 0 & 0 & 0 & 0 & 0 & 0 \\ 0 & 0 & 0 & 0 & 0 & 0 & 0 & 0 & 0 & 0 & 0 & 0 & 2 & 0 & 0 & 0 & 0 & 0 \\ 0 & 0 & 0 & 0 & 0 & 0 & 0 & 0 & 0 & 0 & 0 & 0 & 0 & 2 & 0 & 0 & 0 & 0 \\ 0 & 0 & 0 & 0 & 0 & 0 & 0 & 0 & 0 & 0 & 0 & 0 & 0 & 0 & 4 & 0 & 0 & 0 \\ 0 & 0 & 0 & 0 & 0 & 0 & 0 & 0 & 0 & 0 & 0 & 0 & 0 & 0 & 0 & 4 & 0 & 0 \\ 0 & 0 & 0 & 0 & 0 & 0 & 0 & 0 & 0 & 0 & 0 & 0 & 0 & 0 & 0 & 0 & 4 & 0 \\ 0 & 0 & 0 & 0 & 0 & 0 & 0 & 0 & 0 & 0 & 0 & 0 & 0 & 0 & 0 & 0 & 0 & 4 \end{bmatrix} \end{array} \tag{10}$$

$$
Laplacian = \begin{array}{c} \\ v_1 \\ v_2 \\ v_3 \\ v_4 \\ v_5 \\ v_6 \\ v_7 \\ v_8 \\ v_9 \\ v_{10} \\ v_{11} \\ v_{12} \\ v_{13} \\ v_{14} \\ v_{15} \\ v_{16} \\ v_{17} \\ v_{18} \end{array}
\begin{array}{c}
\begin{array}{cccccccccccccccccc} v_1 & v_2 & v_3 & v_4 & v_5 & v_6 & v_7 & v_8 & v_9 & v_{10} & v_{11} & v_{12} & v_{13} & v_{14} & v_{15} & v_{16} & v_{17} & v_{18} \end{array} \\
\left[\begin{array}{cccccccccccccccccc}
1 & 0 & 0 & 0 & 0 & 0 & 0 & 0 & 0 & 0 & 0 & 0 & 0 & 0 & -1 & 0 & 0 & 0 \\
0 & 1 & 0 & 0 & 0 & 0 & 0 & 0 & 0 & 0 & 0 & 0 & 0 & 0 & 0 & 0 & 0 & 0 \\
0 & 0 & 1 & 0 & 0 & 0 & 0 & 0 & 0 & 0 & 0 & 0 & 0 & 0 & -1 & -1 & 0 & 0 \\
0 & 0 & 0 & 1 & 0 & 0 & 0 & 0 & 0 & 0 & 0 & 0 & 0 & 0 & 0 & 0 & 0 & 0 \\
0 & 0 & 0 & 0 & 1 & 0 & 0 & 0 & 0 & 0 & 0 & 0 & 0 & 0 & 0 & 0 & 0 & -1 \\
0 & 0 & 0 & 0 & 0 & 1 & 0 & 0 & 0 & 0 & 0 & 0 & 0 & 0 & 0 & -1 & 0 & 0 \\
0 & 0 & 0 & 0 & 0 & 0 & 1 & 0 & 0 & 0 & 0 & 0 & 0 & 0 & 0 & 0 & 0 & 0 \\
0 & 0 & 0 & 0 & 0 & 0 & 0 & 1 & 0 & 0 & 0 & 0 & -1 & 0 & 0 & 0 & 0 & 0 \\
0 & 0 & 0 & 0 & 0 & 0 & 0 & 0 & 1 & 0 & 0 & 0 & 0 & -1 & 0 & 0 & 0 & 0 \\
0 & 0 & 0 & 0 & 0 & 0 & 0 & 0 & 0 & 1 & 0 & 0 & 0 & -1 & 0 & 0 & 0 & 0 \\
0 & 1 & 0 & 0 & 0 & 0 & 0 & 0 & 0 & 0 & 2 & 0 & 0 & 0 & 0 & 0 & -1 & 0 \\
0 & 0 & 0 & 1 & 0 & 0 & 0 & 0 & 0 & 0 & 0 & 2 & 0 & 0 & 0 & 0 & 0 & -1 \\
0 & 0 & 0 & 0 & 0 & 0 & 0 & -1 & 0 & 0 & 0 & 0 & 2 & 0 & -1 & 0 & 0 & 0 \\
0 & 0 & 0 & 0 & 0 & 0 & 0 & 0 & -1 & -1 & 0 & 0 & 0 & 2 & 0 & 0 & 0 & 0 \\
-1 & 0 & 0 & 0 & 0 & 0 & -1 & 0 & 0 & 0 & 0 & 0 & -1 & 0 & 4 & 0 & -1 & 0 \\
0 & 0 & -1 & 0 & 0 & -1 & 0 & 0 & 0 & 0 & 0 & 0 & 0 & 0 & 0 & 4 & -1 & -1 \\
0 & 0 & 0 & 0 & 0 & 0 & 0 & 0 & 0 & 0 & -1 & 0 & 0 & 0 & -1 & -1 & 4 & -1 \\
0 & 0 & 0 & 0 & -1 & 0 & 0 & 0 & 0 & 0 & 0 & -1 & 0 & 0 & 0 & -1 & -1 & 4
\end{array}\right]
\end{array}
\tag{11}
$$

For equation $Laplacian \bullet x = 0$, its general solution is shown in Eq. (12). In this equation, α_1 and α_2 are solution vectors of the fundamental system, and nodes corresponding to their nonzero elements compose a subsystem. For the Digraph shown in Fig. 5, the solution of Eq. (12) is shown in Eq. (13) and Eq. (14). Based on this, two irrelevant subsystems can be identified, the node set of one is $\{v_1, v_2, v_3, v_4, v_5, v_6, v_7, v_8, v_{11}, v_{12}, v_{13}, v_{14}, v_{15}, v_{16}, v_{17}, v_{18}\}$ and that of the other is $\{v_9, v_{10}, v_{12}\}$, as shown in Fig. 6.

$$x = A\alpha_1 + B\alpha_2 \tag{12}$$

Where A and B are real numbers.

$$
\begin{array}{c}
\begin{array}{cccccccccccccccccc} v_1 & v_2 & v_3 & v_4 & v_5 & v_6 & v_7 & v_8 & v_9 & v_{10} & v_{11} & v_{12} & v_{13} & v_{14} & v_{15} & v_{16} & v_{17} & v_{18} \end{array} \\
\alpha_1 = \left[\begin{array}{cccccccccccccccccc} 1 & 1 & 1 & 1 & 1 & 1 & 1 & 1 & 0 & 0 & 1 & 0 & 1 & 1 & 1 & 1 & 1 & 1 \end{array}\right]^{\top}
\end{array}
\tag{13}
$$

$$\alpha_2 = \begin{matrix} v_1 & v_2 & v_3 & v_4 & v_5 & v_6 & v_7 & v_8 & v_9 & v_{10} & v_{11} & v_{12} & v_{13} & v_{14} & v_{15} & v_{16} & v_{17} & v_{18} \\ \left[0 \right. & 0 & 0 & 0 & 0 & 0 & 0 & 0 & 1 & 1 & 0 & 1 & 0 & 0 & 0 & 0 & 0 & \left. 0\right]^{\top} \end{matrix} \quad (14)$$

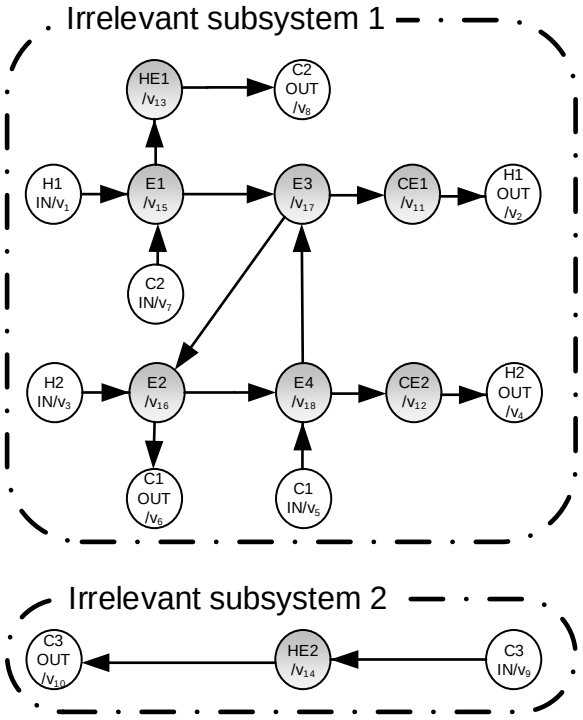

Fig. 6 Two irrelevant subsystems of the HEN shown in Fig. 4 and Fig. 5

4. Disturbance transmission analysis model

The stream parameters often fluctuate in chemical production due to internal or external interferences. For example, the catalyst deactivation can lead to the fluctuation of the reactor's effluent, and the weather change affects the working conditions of the distillation column and the heat exchanger, consequently affecting product quality and energy consumption. Parameter fluctuations are acceptable within a specific range, but once the design margin is exceeded, they will have a negative impact on the system. For highly coupled systems, parameter fluctuations can be transmitted among devices. It is significant to explore how the parameter

fluctuations shift in the HEN and establish a model to evaluate their impact. In this section, adjacency and reachability matrices will be used to determine whether the fluctuation is reachable. A systematic model is established to explore the fluctuation transfer path based on the node information stored in the adjacency matrix.

4.1 Excitation and its calculation

For a highly coupled HEN, the Excitation is used to measure the degree of coupling among heat exchangers and the influence of parameter fluctuations on the system. High Excitation represents a high coupling degree among heat exchangers and impacts the whole system significantly.

Fluctuation transmission path

To explore the parameter fluctuations' influence on the HEN, it is necessary to clarify the fluctuation transmission path first. The fluctuation transmission from the decision variable to the state variable is the fluctuation transmission path (Linnhoff and Kotjabasakis, 1986). The decision variable refers to the variable directly disturbed, and the state variable refers to the variable affected by the decision variables (Yang et al., 1996). Zhao and Liu (2022) defined the path/direction, key equipment, and fluctuation transmission path, and clarified the calculation formula and law of single-variable and multi-variable load migration. The fluctuation transmission path is equivalent to the heat flow path (Kemp, 2007), which refers to the route connecting the heaters and coolers, including all the heat exchangers in the route.

However, in practical chemical systems, the possible paths of load and fluctuation transfer are not single and are limited by the heat transfer area. The model proposed by Zhao and Liu (2022) cannot automatically identify all possible fluctuation transmission paths. This work will improve this method to identify all possible paths automatically.

The basic rules for targeting all fluctuation transmission paths are as follows:

1) A heat flow path from the fluctuation parameter to a stream's outlet is a potential fluctuation transmission path;
2) The heat flow path can only propagate in the stream's flow direction and cannot propagate reversely;
3) There is no heat load loop in the fluctuation transmission path since the heat load loop always satisfies the node enthalpy balance (Shivakumar and Narasimhan, 2002). In other words, each heat exchanger in a fluctuation transmission path appears only once.

The system shown in Fig. 4 will be an illustrative example to analyze the fluctuation migration. When the inlet temperature of H1 fluctuates, the fluctuation migration path is shown in Fig. 7.

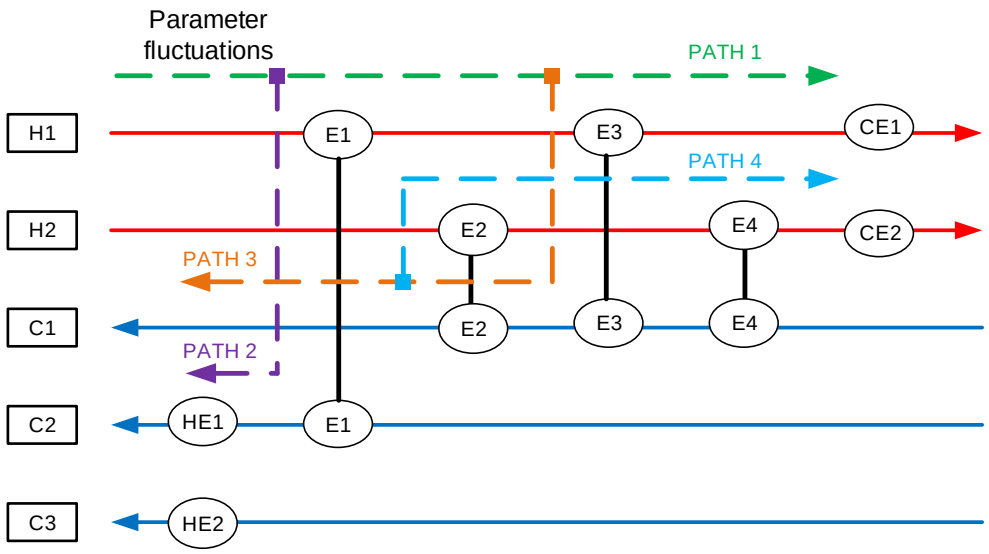

Fig. 7 The fluctuation transmission path of the system shown in Fig. 4 when H1's inlet temperature fluctuates

Global Sensitivity

The parameter fluctuation has a different impact on the heat exchangers of the fluctuation transmission path. The sensitivity and sensitivity coefficient are introduced as weights to measure the impact accurately. The sensitivity coefficient reflects the degree of the state variable change with the decision variable. If the state variable is very sensitive to the fluctuation of the decision variable, the sensitivity coefficient would be high, and it is challenging to keep stable operations. For a system with *n* decision variables and *m* state variables, the state and decision variables are represented by *s* and *d*, respectively. The first-order sensitivity of the state variable relative to the decision variable is expressed in Eq. (15).

$$Sensitivity_d^s = \frac{\Delta s / s^*}{\Delta d / d^*} = \left(\frac{\Delta s}{\Delta d}\right)_{d^*} \Big/ \frac{s^*}{d^*} \tag{15}$$

Where, Δs and Δd represent the magnitude of variable change, s^* and d^* represent the stable value of the variable. When $\Delta d \to 0$, the sensitivity coefficient equals $\left(\frac{\Delta s}{\Delta d}\right)_{d^*}$. The matrix of the multi-dimensional sensitivity coefficient is shown in Eq. (16).

$$\mathbf{SC}_{\mathbf{D}}^{\mathbf{S}} = \begin{bmatrix} \frac{\partial s_1}{\partial d_1} & \cdots & \frac{\partial s_n}{\partial d_1} \\ \vdots & \ddots & \vdots \\ \frac{\partial s_m}{\partial d_1} & \cdots & \frac{\partial s_m}{\partial d_n} \end{bmatrix}_{m \times n} \tag{16}$$

Where $\mathbf{S}$ and $\mathbf{D}$ are the state and the decision vectors, respectively, as shown in Eqs. (17) and (18).

$$\mathbf{S} = \begin{bmatrix} s_1 & s_2 & \cdots & s_m \end{bmatrix}_m \tag{17}$$

$$\mathbf{D} = \begin{bmatrix} d_1 & d_2 & \cdots & d_n \end{bmatrix}_n \tag{18}$$

Each heat exchange unit's heat balance and heat transfer are described by Eq. (19) and Eqs. (20)-(21).

$$Eq_{balance} = F_C Cp_C \left(t_C^{out} - t_C^{in}\right) - F_H Cp_H \left(t_H^{in} - t_H^{out}\right) = 0 \tag{19}$$

$$Eq_{transfer} = Q - Area \bullet K \bullet LMTD \tag{20}$$

$$LMTD = \frac{\left(t_H^{in} - t_C^{out}\right) - \left(t_H^{out} - t_C^{in}\right)}{\ln\left[\left(t_H^{in} - t_C^{out}\right) / \left(t_H^{out} - t_C^{in}\right)\right]} \tag{21}$$

Where F denotes the flow rate, $kg \cdot h^{-1}$; Cp is the heat capacity of streams, $kW \cdot h \cdot kg^{-1} \cdot ℃^{-1}$; Q represents the heat load, kW; K is the total heat transfer coefficient, $kW \cdot m^{-}$

$^{2}\cdot℃^{-1}$; *Area* is the heat transfer area, m^2; *LMTD* is the logarithmic mean heat exchange temperature difference, ℃, and can be calculated by Eq. (21); *t* stands for the stream temperature, ℃; superscripts *H* and *C* represent the hot and cold streams; superscripts *in* and *out* denote the inlet and outlet.

For a HEN with *i* heat exchange units, there are *2i* heat balance and heat transfer equations, as shown in Eq. (22). The multi-dimensional sensitivity coefficient matrix can be calculated by Eq. (23).

$$\mathbf{Eq} = f\left(\mathbf{S},\mathbf{D}\right)_{2i} = 0 \tag{22}$$

$$\mathbf{SC}_{\mathbf{D}}^{\mathbf{S}} = -\left(\frac{\partial \mathbf{Eq}}{\partial \mathbf{S}}\right)^{-1}\left(\frac{\partial \mathbf{Eq}}{\partial \mathbf{D}}\right) \tag{23}$$

Where $\mathbf{SC}_{\mathbf{D}}^{\mathbf{S}}$ denotes the sensitivity coefficient matrix, and $\left(\frac{\partial \mathbf{Eq}}{\partial \mathbf{S}}\right)^{-1}$ denotes the left inverse matrix of $\left(\frac{\partial \mathbf{Eq}}{\partial \mathbf{S}}\right)$.

Excitation and Its Definition

The Excitation on a single stream is the product of two terms, the sum of the sensitivity coefficients (absolute values) of all heat exchangers' outlet temperatures and the length of the parameter fluctuation interval. The sum of all streams' Excitation is the HEN's Excitation.

In the HEN, temperature fluctuation is mainly considered. Suppose that a HEN has *P* streams, the fluctuation transmission path corresponding to the inlet parameter of stream *i* is stored in the nested sequence $\mathbf{R_i}$, $\mathbf{R_i}$ = [$\mathbf{r}_1$, $\mathbf{r}_2$,...], and the fluctuation

interval of stream *i*'s inlet parameter is $\mathbf{W}_i$. Taking each stream's inlet temperature (T_i^{in}) as the decision variable and the outlet temperature (t_k) of the downstream heat exchanger *k* along the heat flow path as the state variable, the Excitation of the HEN is shown in Eq. (24).

$$Excitation = \sum_{i=1}^{P} \mathbf{W}_i \sum_{j=1}^{len(\mathbf{R}_i)} \sum_{k \text{ in } \mathbf{R}_i(\mathbf{r}_j)} \left| \frac{\partial t_k}{\partial T_i^{in}} \right| \tag{24}$$

Where *len()* represents a function to obtain the length of the parameter fluctuation interval.

Based on the structure information stored in the adjacency matrix, Eqs. (19)-(21), and Eqs. (23)-(24), the HEN's Excitation can be calculated.

4.2 Algorithm for calculating Excitation

The fluctuation transmission paths shown in the grid diagram can be illustrated in the Digraph. For example, Fig. 7 can be transmitted into Fig. 8. The nodes of all fluctuation transmission paths are in the same independent subsystem. The basic rules for searching all the transmission paths are transformed into the following description in terms of graph theory:

1) All paths from the initial node to the target node are a potential fluctuation transmission path;
2) The path must be connected following the direction of the directed edge; the out-degree and in-degree of the stream's initial node are 1 and 0, respectively, while those of the stream's target node are 0 and 1. For the nodes inside each path, the in-degree and out-degree are 1.

3) Loops do not exist in the path; each node is only accessed once.

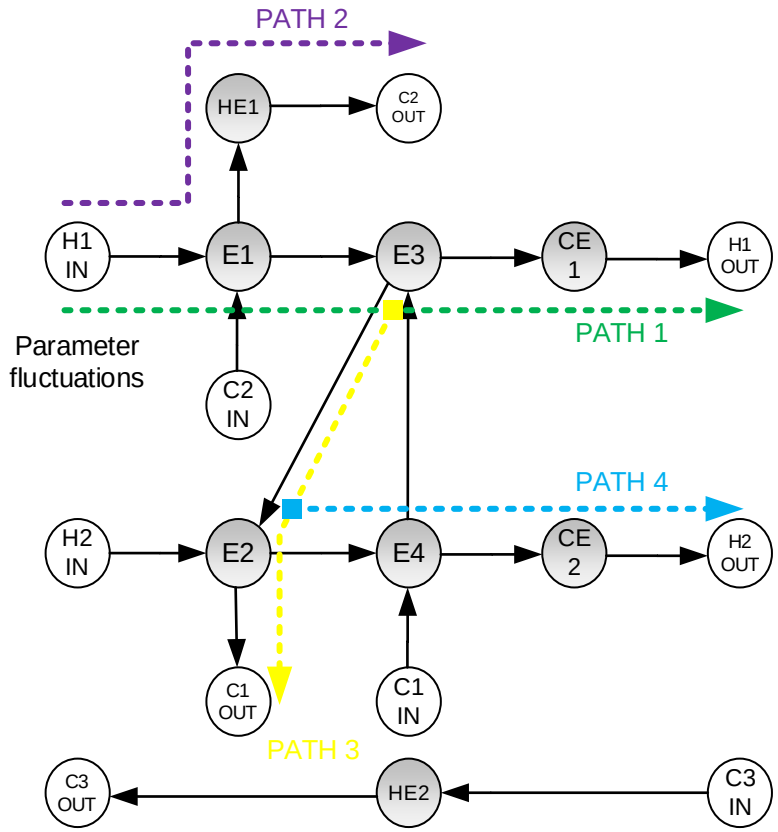

Fig. 8 The fluctuation transmission path represented in a directed graph

In graph theory, the simple path of a Digraph is defined as that with all nodes different in the connection direction of the edges. The simple path exists in the same connected component. Searching for the HEN's fluctuation transmission path is equivalent to targeting all the simple paths of the Digraph, with the stream's initial as the start node of the fluctuation transmission path and the stream's target as the end node.

Another key to identifying the Excitation is calculating the sensitivity coefficient matrix, whose element is the process equations' partial derivatives over the

decision and state variables. In this work, the inlet temperature of each stream is taken as the decision variable, and the outlet temperature of each heat exchanger is the state variable; each heat exchanger's heat load and utilities' inlet/outlet temperatures are constant.

For any heat exchange unit, the partial derivatives of Eq. (20) over t_H^{in}, t_H^{out}, t_C^{in}, and t_C^{out}, are shown in Eqs. (25)-(28). Table 1 summarizes the partial derivative calculation equations over decision variables and state variables.

$$\frac{\partial Eq_{transfer}}{\partial t_H^{in}} = -KArea / \log\left(\frac{-t_C^{out}+t_H^{in}}{-t_C^{in}+t_H^{out}}\right) + \frac{KArea\times\left(t_C^{in}-t_C^{out}+t_H^{in}-t_H^{out}\right)}{\left(-t_C^{out}+t_H^{in}\right)\times\log\left(\frac{-t_C^{out}+t_H^{in}}{-t_C^{in}+t_H^{out}}\right)^2} \tag{25}$$

$$\frac{\partial Eq_{transfer}}{\partial t_H^{out}} = -KArea / \log\left(\frac{-t_C^{out}+t_H^{in}}{-t_C^{in}+t_H^{out}}\right) - \frac{KArea\times\left(t_C^{in}-t_C^{out}+t_H^{in}-t_H^{out}\right)}{\left(-t_C^{in}+t_H^{out}\right)\times\log\left(\frac{-t_C^{out}+t_H^{in}}{-t_C^{in}+t_H^{out}}\right)^2} \tag{26}$$

$$\frac{\partial Eq_{transfer}}{\partial t_C^{in}} = -KArea / \log\left(\frac{-t_C^{out}+t_H^{in}}{-t_C^{in}+t_H^{out}}\right) + \frac{KArea\times\left(t_C^{in}-t_C^{out}+t_H^{in}-t_H^{out}\right)}{\left(-t_C^{in}+t_H^{out}\right)\times\log\left(\frac{-t_C^{out}+t_H^{in}}{-t_C^{in}+t_H^{out}}\right)^2} \tag{27}$$

$$\frac{\partial Eq_{transfer}}{\partial t_C^{out}} = -KArea / \log\left(\frac{-t_C^{out}+t_H^{in}}{-t_C^{in}+t_H^{out}}\right) - \frac{KArea\times\left(t_C^{in}-t_C^{out}+t_H^{in}-t_H^{out}\right)}{\left(-t_C^{out}+t_H^{in}\right)\times\log\left(\frac{-t_C^{out}+t_H^{in}}{-t_C^{in}+t_H^{out}}\right)^2} \tag{28}$$

Table 1 The partial derivative calculation equations over decision variables and state variables

	Location of the heat exchange unit	Decision variable	Balance equation				heat-transfer equation			
			$T_{H,in}$	$T_{H,out}$	$T_{C,in}$	$T_{C,out}$	$T_{H,in}$	$T_{H,out}$	$T_{C,in}$	$T_{C,out}$
$\frac{\partial Eq}{\partial \mathbf{D}}$	The first unit in the path	Cold stream's inlet temperature	0	0	$-FCP_C$	0	0	0	Eq.(27)	0
		Hot stream's inlet temperature	FCP_H	0	0	0	Eq.(25)	0	0	0
		The inlet temperature of cold and hot streams	FCP_H	0	$-FCP_C$	0	Eq.(25)	0	Eq.(27)	0
	Not the first unit in the path		0	0	0	0	0	0	0	0
$\frac{\partial Eq}{\partial \mathbf{S}}$	The first unit in the path	Cold stream's inlet temperature	FCP_H	FCP_H	0	$-FCP_C$	Eq.(25)	Eq.(26)	0	Eq.(28)
		Hot stream's inlet temperature	0	FCP_H	$-FCP_C$	$-FCP_C$	0	Eq.(26)	Eq.(27)	Eq.(28)
		The inlet temperature of cold and hot streams	0	FCP_H	0	$-FCP_C$	0	Eq.(26)	0	Eq.(28)
	Not the first unit in the path		FCP_H	FCP_H	$-FCP_C$	$-FCP_C$	Eq.(25)	Eq.(26)	Eq.(27)	Eq.(28)

The Depth-First Search (DFS) algorithm (Tarjan, 1971), a tool developed for traversing trees or graphs and also having the capacity to explore the branches of the tree as deep as possible, will be employed to search all possible fluctuation transmission paths of the HEN before calculating the Excitation. The maximum stack depth of the algorithm is the height of the tree (*h*), the space complexity is O(*h*), and the time complexity, O(*n*), is only related to the number of nodes (*n*). The flow chart of the DFS algorithm is shown in Fig. 9.

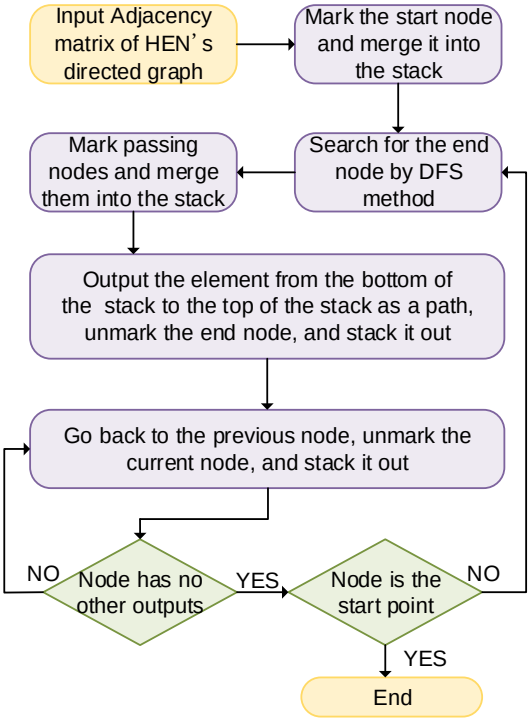

Fig. 9 DFS algorithm flow chart

The calculation process of the HEN's Excitation is as follows:

Step 1. Input the Initial data. The input data include the stream's temperature, heat capacity flow rate, fluctuation range, utility temperature, etc.

Step 2. Allocate nodes to streams. Assign the nodes and serial numbers to each stream's initial and target, the utility heat exchanger, and the heat exchanger according to the structural information of the feasible solution and the order and flow direction of the stream. The serial number of each node is unique, and each heat exchanger is taken as one node.

Step 3. Search the fluctuation transmission path. The HEN's topological information is stored in the adjacency matrix, and the reachable matrix is calculated according to the pseudo-code shown in Table A. 1. Each stream's initial and target are set as the starting and end nodes. If these two nodes are not accessible, the empty set is output; otherwise, all potential fluctuation transmission paths are searched by the DFS algorithm shown in Fig. 9.

Step 4. Calculate the sensitivity coefficient matrix.

1) Calculate the *KArea* of each heat exchanger according to Eq. (20);
2) Calculate the partial derivative matrix of the process equation vector over the decision variables according to Table 1;
3) Calculate the partial derivative matrix of the process equation vector over the state variables according to Table 1 and Eqs. (25)-(28);
4) Calculate the sensitivity coefficient matrix according to Eq. (23).

Step 5. Calculate the Excitation. Calculate the Excitation of the whole HEN according to the fluctuation transmission path, the sensitivity coefficient matrix obtained in the previous steps, and Eq. (24).

Based on the above steps and Eqs. (20) and (23)-(28), the Excitation can be automatically calculated and optimized as one of the objectives.

5. Superstructure Model for Optimizing Excitation and Utility Consumption

5.1 Multiple-objective superstructure model

The improved superstructure model established in this study is based on the split-less stage-wise superstructure proposed by Yee et al. (1990). For a system with N_H hot streams and N_C cold streams, the number of superstructure's stages (N_S) equals $\max\{N_H, N_C\}$, and the stream mixing is assumed to be isothermal mixing. This superstructure model is a non-convex MINLP problem with multiple locally optimal solutions, and its optimization is challenging.

Unlike the model proposed by Yee et al. (1990), which adopted the total cost as one of its objectives, this model adopts the energy cost as one of its objectives instead. The Excitation and investment cost generally increases with the number of process stream's heat exchangers while the utility cost decreases. The greater the Excitation, the worse the ability of the HEN to resist parameter fluctuations. On the other hand, the total cost will decrease first and then increase along with the Excitation, as shown in Fig. 10. In solving the multi-objective MINLP model, a certain number of bad solutions exist in the population. When the total cost is taken as an objective function, the Pareto solution aggregation chooses the one with smaller Excitation under the same cost, and this makes it difficult for the population to search or even unable to explore the solution on both sides of the extreme point, and consequently affecting the global optimization. Considering the globality, the energy or investment cost as the optimization objective is far better than the total

cost. With the energy cost and Excitation taken as the optimization objectives and specific strategy used to select the appropriate solution from the Pareto solution set, the total cost can also be approached or minimized.

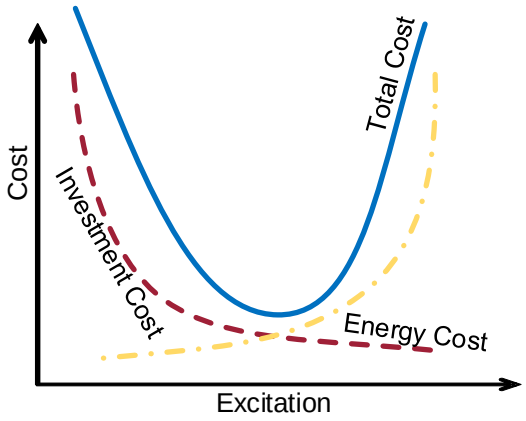

Fig. 10 The cost versus Excitation chart

Objectives

$$\min Excitation = \sum_{i=1}^{P} \mathbf{W}_i \sum_{j=1}^{len(\mathbf{R}_i)} \sum_{k \text{ in } \mathbf{R}_i(\mathbf{r}_j)} \left| \frac{\partial t_k}{\partial T_i^{in}} \right| \tag{29}$$

$$\min Energy = \sum_{i=1}^{N_H} Q_{CU,i} + \sum_{j=1}^{N_C} Q_{HU,j} \tag{30}$$

Constraints

1) Heat balance of streams

$$\left(T_i^{in} - T_i^{out}\right) \bullet F_i \bullet Cp_i = \sum_{k=1}^{N_S} \sum_{j=1}^{N_C} Q_{i,j,k} + Q_{CU,i} \quad i \in N_H \tag{31}$$

$$\left(T_j^{out} - T_j^{in}\right) \bullet F_j \bullet Cp_j = \sum_{k=1}^{N_S} \sum_{i=1}^{N_H} Q_{i,j,k} + Q_{HU,j} \quad j \in N_C \tag{32}$$

2) Stage-wise superstructure thermal equilibrium

$$\begin{aligned} Q_{i,j,k} &= F_i \bullet Cp_i \bullet \left(t_{i,k}^{in} - t_{i,k}^{out}\right) \\ &= F_j \bullet Cp_j \bullet \left(t_{j,k}^{out} - t_{j,k}^{in}\right) \end{aligned} \quad i \in N_H, j \in N_C, k \in N_S \tag{33}$$

3) Heat balance of heat exchangers

$$Q_{CU,i} = F_i \bullet Cp_i \bullet \left(t_{i,N_S}^{out} - T_i^{out} \right) \quad i \in N_H \tag{34}$$

$$Q_{HU,j} = F_j \bullet Cp_j \bullet \left(T_j^{in} - t_{j,1}^{in} \right) \quad j \in N_C \tag{35}$$

4) Temperature feasibility

$$t_{i,k} \geq t_{i,k+1} \quad i \in N_H, k \in N_S - 1 \tag{36}$$

$$t_{j,k} \geq t_{j,k+1} \quad j \in N_C, k \in N_S - 1 \tag{37}$$

$$t_{i,N_S}^{out} \geq T_i^{out} \quad i \in N_H \tag{38}$$

$$T_j^{out} \geq t_{j,1}^{out} \quad j \in N_C \tag{39}$$

5) Heat transfer temperature difference

$$t_{i,k}^{in} - t_{i,k}^{out} \geq \Delta t_{\min} \quad i \in N_H, j \in N_C, k \in N_S \tag{40}$$

$$t_{i,k}^{out} - t_{j,k}^{in} \geq \Delta t_{\min} \quad i \in N_H, j \in N_C, k \in N_S \tag{41}$$

6) Number of heat exchangers

$$\sum_{i=1}^{N_H} Z_{i,j,k} \leq 1 \quad j \in N_C, k \in N_S \tag{42}$$

$$\sum_{j=1}^{N_C} Z_{i,j,k} \leq 1 \quad i \in N_H, k \in N_S \tag{43}$$

7) Binary constraint

$$Z_{i,j,k} = \begin{cases} 0 & \text{No heat transfer between streams } i \text{ and } j \text{ in stage } k \\ 1 & \text{Heat transfer exsists between streams } i \text{ and } j \text{ in stage } k \end{cases} \quad i \in N_H, j \in N_C, k \in N_S \tag{44}$$

Where T represents the stream temperature, ℃, t is the stage temperature, ℃; F is the flow rate, kg·h^{-1}; Cp stands for the heat capacity of streams , kW·h·kg^{-1}·℃$^{-1}$; Q is the heat load, kW; Z denotes a binary (0-1) variable, indicating whether the

heat exchanger exists or not. Subscripts H and C represent the hot and cold streams, S represents the stage, subscripts CU and HU denote the cooling and heating utilities. Superscript *in* and *out* stand for the inlet and outlet.

This model takes Excitation and utility consumption as optimization objectives. With the structure and energy consumption optimized, the obtained HEN will have strong resistance to parameter fluctuations and low energy consumption.

5.2 Improved NSGA-II algorithm

The traditional multi-objective optimization algorithm generally converts multiple objective functions into one function by a relatively reasonable model. For the optimization in terms of Excitation and utility consumption, there is no clear mathematical relationship between the decision variable and the Excitation, and it is not easy to find a reasonable model to combine two objective functions into one. Hence, the traditional optimization algorithm cannot be used.

NSGA-II (Deb et al., 2002) is an extraordinary multi-objective optimization algorithm and will be improved to optimize the proposed multi-objective MINLP model.

5.2.1 Basic NSGA-II Algorithm

The basic NSGA-II includes five steps.

Step 1. Generate the initial population. The decision variables are randomly generated, and the fitness function is calculated. The initial solution is non-dominated and sorted according to the value of the fitness function, and the crowding distance is calculated according to Eq. (45). The crowding distance is the normalized Manhattan distance of the two points before and after the solution.

If the point corresponds the solution with the maximum or minimum objective in the population, the crowding degree is positive infinity.

$$Crowding_i = \left| \frac{obj_{1,i-1} - obj_{1,i+1}}{obj_{1,\max} - obj_{1,\min}} \right| + \left| \frac{obj_{2,i-1} - obj_{2,i+1}}{obj_{2,\max} - obj_{2,\min}} \right| \tag{45}$$

Step 2. Selection, crossover, and mutation. Firstly, two parents are selected according to roulette and binary championships, and half of their $Z_{i,j,k}$ will be exchanged to generate offspring. There is a 50 % probability of mutation in the offspring, which is to redistribute the heat exchanger to one stage of the superstructure. Then, the fitness function of the offspring can be calculated with Eq. (29) and Eq. (30).

Step 3. Elite solution strategy. The parent and the offspring are placed in the same population bank, the non-dominated rapid sorting is performed, and the crowding degree is calculated. The top 50 % is selected as the parent of the next generation.

Step 4. Other operator improvement strategies. Implement the population migration and gene pool strategies, and trigger the decapitation and disaster strategies under appropriate conditions. The specific descriptions will be introduced in Section 5.2.3.

Step 5. Iteration and convergence. Repeat **Steps 2-4** until the number of iterations or convergence conditions are satisfied.

NSGA-II has the following advantages:

1) It does not require a precise mathematical relationship between the objective functions and the decision variables;
2) There is no limitation on linearity, convexity, and continuity of the problem, and thus it can deal with highly complex models and constraints;
3) Multiple objectives do not need to be converted into one, and the solution can be evaluated based on the non-dominated rank and crowding distance.
4) The data structure of the decision variable ($Z_{i,j,k}$) is suitable for the NSGA-II algorithm's binary coding, crossover, and mutation.

5.2.2 Strategies for Generating Feasible Solutions

Since the HEN's superstructure model has extremely harsh constraints, the randomly generated initial solution is generally infeasible and cannot lead to optimal solutions. Strategies are proposed and employed to ensure that sufficient feasible initial solutions can be generated.

Forbidden Matching Strategy

In the superstructure model, there are three possible temperature relationships between two streams, as shown in Fig. 11. In Fig. 11 (a), the T-H line of the hot stream lies above that of the cold stream; the hot and cold streams conform to the temperature constraints and can exchange heat. In Fig. 11 (b), the two T-H lines intersect, the two streams partly meet the temperature constraints, and the heat exchange in the temperature interval above the intersecting point is feasible. In Fig.

11 (c), the T-H line of the cold stream lies above that of the hot stream, and their match is forbidden, that is, $Z_{i,j,k}$ equals 0, and the corresponding match can be prohibited to improve the optimization efficiency. Based on the above analysis, the inequality constraints of Eqs. (40) and (41) is transformed into the equality constraints shown in Eq. (46).

$$Z_{i,j,k} = Z_{i,j,k} \times \frac{\max(t_{i,k}^{in} - t_{j,k}^{out} - \Delta t_{\min}, 0)}{t_{i,k}^{in} - t_{j,k}^{out} - \Delta t_{\min}} \quad i \in N_H, j \in N_C, k \in N_S \tag{46}$$

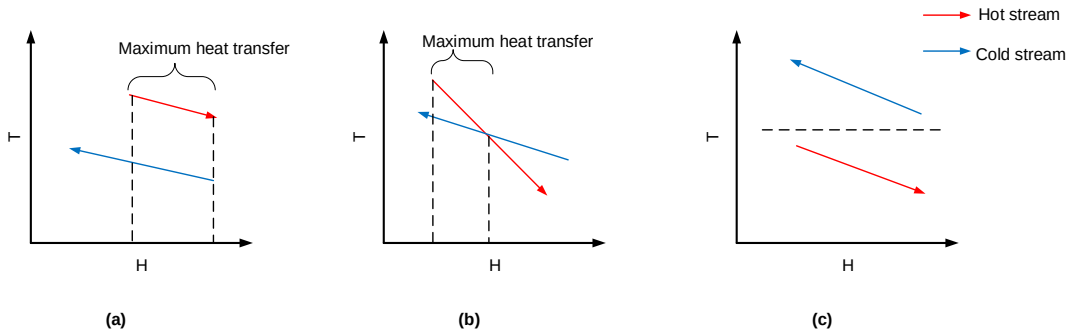

Fig. 11 Temperature relationship and maximum heat transfer of hot and cold streams

Although the prohibition of the matchings cannot guarantee that all solutions are feasible, it can remove a large number of infeasible solutions in the calculation, improve the quality of solutions, and provide a foundation for evolutionary computation.

Maximum Energy Matching Strategy

In the superstructure model, there is a mutual restraint between heat transfer load and temperature constraints. The heat exchanger load generated randomly may violate the temperature constraints. Different from the transshipment model with the goal of minimizing matching (Papoulias and Grossmann, 1983), the maximum

energy matching strategy developed in this study achieves the goal by maximizing the heat load and dynamically updating constraints, instead of directly optimizing the number of matches..

The maximum energy matching strategy refers to setting the heat exchanger's load to the maximum value it can exchange. A heat exchanger's feasibility can be classified into two situations: the one shown in Fig. 11 (a) is only constrained by the maximum heat transfer load of the streams, and the situation shown in Fig. 11 (b) is constrained by both the temperature and the maximum heat transfer load. The key for the maximum energy matching to be feasible is to continuously update the streams' inlet and outlet temperatures and the forbidden matching relationships. Since there is only one heat exchanger on each stream in each stage, the heat load computed through the maximum energy matching can fully meet the temperature constraints. After the maximum energy matching is performed for all stages, utility heat exchangers are added to streams whose heat exchange duty is not satisfied.

Based on this strategy, Eq. (33) and Eqs. (36)-(39) are transformed into equality constraints, as shown in Eqs. (47)-(49).

$$Q_{i,j,k}=Z_{i,j,k}\times\min\left(\left(t_{i,k}^{out}-T_j^{in}\right)\bullet F_j\bullet CP_j,\left(t_{j,k}^{in}-T_i^{out}\right)\bullet F_i\bullet CP_i\right)\quad i\in N_H,j\in N_C,k\in N_S \tag{47}$$

$$t_{i,k}^{in}=\begin{cases}T_i^{in} & k=1,i\in N_H\\ T_i^{in}-\sum_{K=1}^{k}\sum_{j=1}^{N_C}Q_{i,j,K}\Big/F_i\bullet CP_i & k\neq 1,i\in N_H,j\in N_C,k\in N_S\end{cases} \tag{48}$$

$$t_{j,k}^{out}=\begin{cases}T_j^{out} & k=1,j\in N_C\\ T_j^{out}-\sum_{K=1}^{k}\sum_{i=1}^{N_H}Q_{i,j,K}\Big/F_j\bullet CP_j & k\neq 1,i\in N_H,j\in N_C,k\in N_S\end{cases} \tag{49}$$

The HEN structure obtained by the maximum energy matching strategy is feasible with the minimum number of heat exchangers. Although only the energy target is considered, the maximum energy matching strategy can reduce the number of heat exchangers, thus saving the investment cost.

5.2.3 Strategies for Improving Operator

Selection strategy

Reasonable selection strategy is the key to the global optimal evolution of the population. The combined roulette and binary tournament strategy are used for individual selection, considering the dominance rank and crowding degree between solutions. The roulette is first used to select the level of parent individuals. For two individuals chosen randomly, the binary tournament is used to identify the better individual as one of the parents. The probability calculation of roulette is shown in Eq. (50).

$$Prob(i) = \frac{\frac{\sum_{k=0}^{len(rank_i)}\left(obj_{1,\max} - obj_{1,k}\right)}{\sum_{j=0}^{len(pop)}\left(obj_{1,\max} - obj_{1,j}\right)} + \frac{\sum_{k=0}^{len(rank_i)}\left(obj_{2,\max} - obj_{2,k}\right)}{\sum_{j=0}^{len(pop)}\left(obj_{2,\max} - obj_{2,j}\right)}}{2} \tag{50}$$

Where *rank* represents the solution set with the same dominance level, and *pop* denotes the entire population.

Decapitation and disaster strategy

The proposed model has a high degree of non-convexity and easily falls into the local optimum in the evolution. When the Pareto solution set does not change in three generations or more, the population cannot produce more diverse individuals through evolution. It will cause individuals with similar genes to mate. This

phenomenon will amplify genetic defects, lead to population diseases, malformations, etc., and further lead to the population's ecological collapse. When the decapitation and disaster strategy is triggered, the Pareto front of the population will be eliminated, and the remaining individuals will be reduced by 50% due to the catastrophe. Randomly generated new individuals supplement the missing individuals. This strategy enables the population evolution to jump out of the local optimum.

Population migration strategy

A population's migration can bring a more abundant number of genes to the population. The population migration strategy requires each generation to have 10% of individuals outflow and the same number for migration. Based on this strategy, the population genes' diversity can be ensured by randomly eliminating and generating 10% of the population individuals.

Gene pool strategy

Whether or not the local optimal solution is the global optimal solution is unknown in the evolution process. A gene pool strategy is established to store the Pareto solution set of each generation during the evolution. When the decapitation and disaster strategy or population migration strategy is triggered, the local optimal solution will no longer participate in the evolution iteration. This strategy can ensure that the population evolution direction is to jump out of the local optimal solution while retaining the local optimal solution's gene and ensuring the global optimal solution not be eliminated. When the evolution reaches the number of iterations

and jumps out of the cycle, the gene pool is merged with the final population to select the final Pareto solution set.

The NSGA-II improved based on the above strategies has better performance in multi-objective optimization of HEN, as it enhances the ability to jump out of local optima as well as the quality of initial solutions. The Pareto front and Utopian solution can be identified efficiently.

5.3 Optimization Procedure

Based on the proposed model, strategies, and the improved NSGA-II algorithm, the HEN can be optimized in order to minimize the Excitation and energy consumption. The overall optimization procedure is shown in Fig. 12.

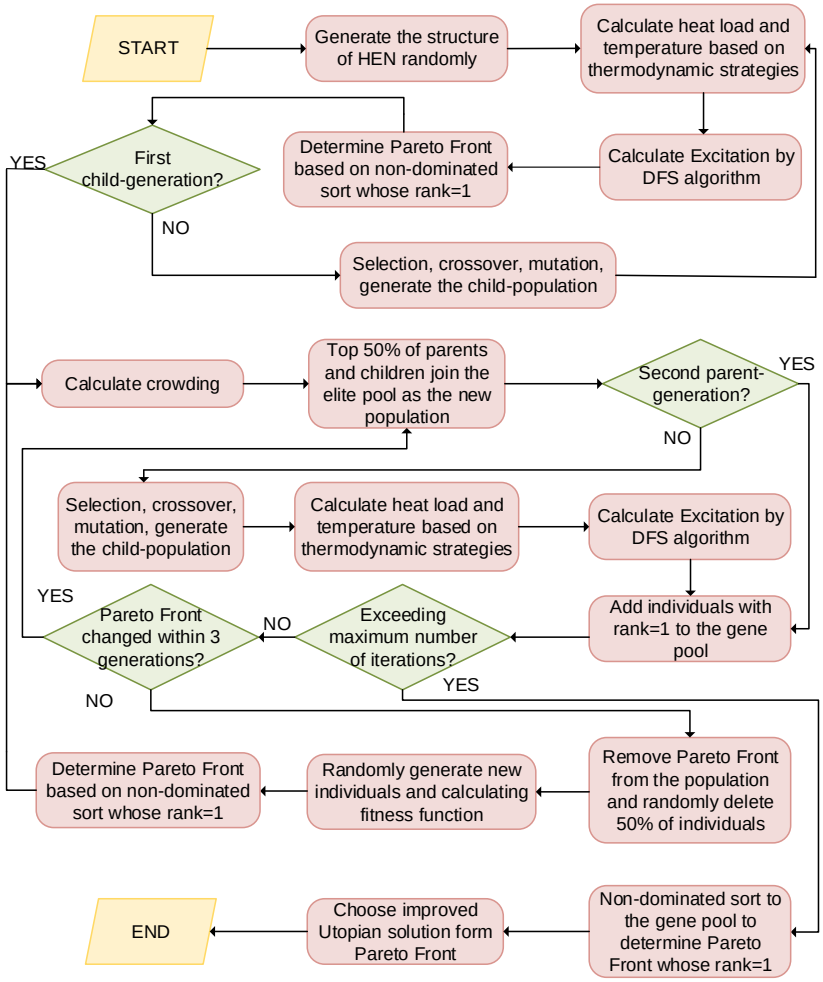

Fig. 12 Overall procedure of the improved NSGA-II

6. Case Study

6.1 Case Description

A coal-to-methanol plant with an annual output of 551,880 tons of refined methanol is studied by the proposed method. The coal-water slurry gasification technology is adopted, and the generated crude syngas is deacidified and washed by low-temperature methanol. The clean syngas is converted into methanol in the methanol synthesis section; the refined methanol is separated in the methanol distillation section, and by-product isobutyl oil is obtained; the H_2S is sent to the

desulfurization recovery section to generate sulfur. The methanol synthesis and distillation sections are the keys of this plant, and the corresponding flowchart is shown in Fig. 13. There are ten hot streams and seven cold streams, and their initial parameters are shown in Table 2. The minimum utility consumption of the system identified by the pinch analysis method is 109,206 kW. When all streams are heated or cooled by utilities, the Excitation is 0.

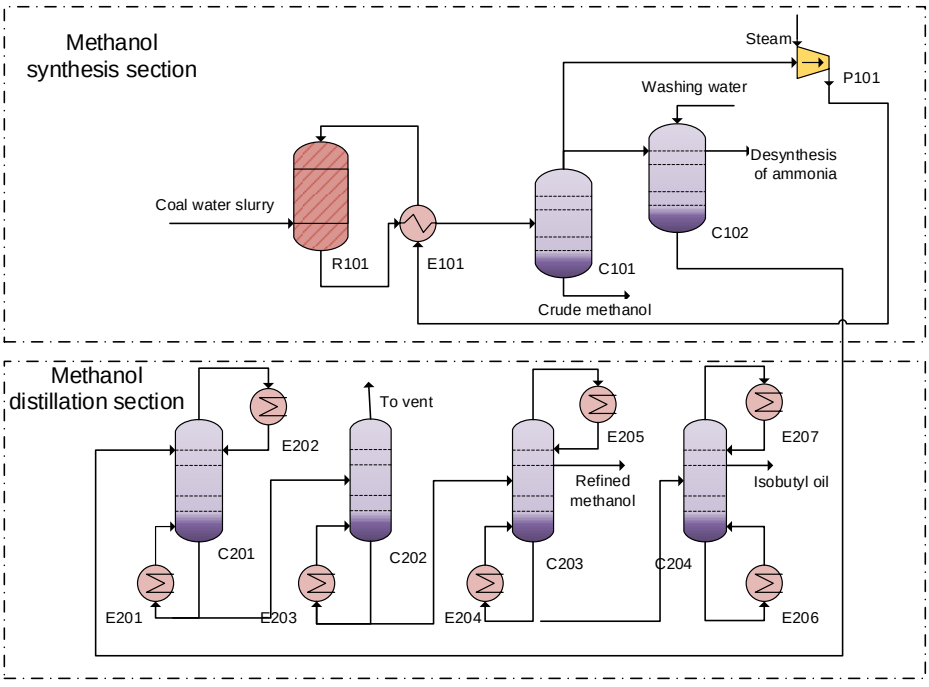

R101 - Coal to methanol reactor
P101 - Compressor
C101 - Methanol separator
C102 - Washing tower

C201 - Pre tower
C202 - Pressurized tower
C203 - Atmospheric tower

C204 - Recovery tower
Heat exchanger - E201 E202
E203 E204 E205 E206 E207

Fig. 13 Flowchart of the methanol synthesis and distillation sections

The parameters of the improved NSGA-II are set as follows:

1) The maximum population evolution is 15 generations;

2) The population size is 100 individuals;

3) The crossover rate is 50%, the mutation probability is 5%, and 30 children are generated per generation.

Based on the proposed model, strategies, and the improved NSGA-II algorithm, HEN's optimization model is built and solved with Python 3.7. The solution is obtained in 101.97 s (The computer processor is Inter (R) Core (TM) i5-9300HCPU@2.40GHz, and the RAM is 8.00G).

Table 2 Data of hot and cold streams

Stream number	Temperature, ℃		Flow rate, $kg \cdot h^{-1}$	Average heat capacity flow rate, $kW \cdot ℃^{-1}$	Heat load, kW
	inlet	outlet			
H1	242	30	279,623	284.67	39,854
H2	72	57	47,000	983.07	14,746
H3	57	54	2,480	28.33	85
H4	125	102	41,978	52.35	1,204
H5	112.6	44	34,800	33.01	2,278
H6	117 .4	112.6	133,000	359,810	35,981
H7	68	53	119,517	2529	37,935
H8	51	31	32,500	27.65	553
H9	69	49	3,502	56.3	1,126
H10	109	40	8,114	9.75	673
C1	43	208	279,623	241.54	39,854
C2	40	61	70,715	63.81	1,340
C3	73	73.8	127,449	20,300	16,240
C4	74.3	89	76,778	81.9	1,204
C5	123	126	171,184	13,090	39,270
C6	109.2	109.3	67,191	359,810	35,981
C7	105	105.1		10,680	1,068

6.2 Pareto Front and Improved Utopian Solution

The obtained minimum energy target and the minimum Excitation target evolution curves are shown in Fig. 14; the Pareto front is shown in Fig. 15.

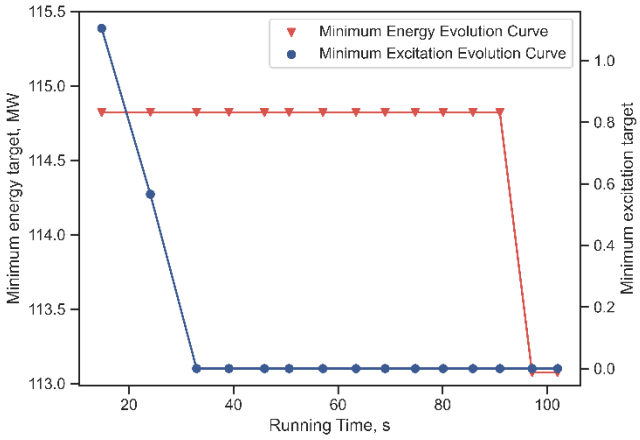

Fig. 14 Optimization objectives' evolution curve

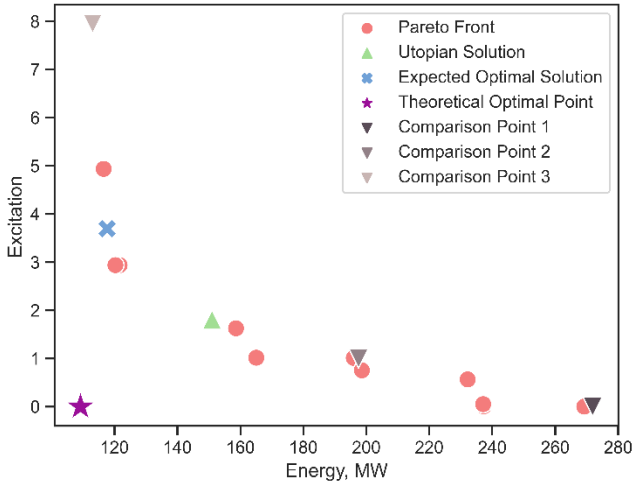

Fig. 15 Pareto Front of the optimization

The Utopian solution refers to the point with the smallest normalized Euclidean distance to the theory optimal point, obj = (109,206kW, 0). Eq. (51) is used to calculate the normalized Euclidean distance.

Considering the Excitation and the energy targets, the ideal solution is not the Utopian solution selected by Eq. (51) but the one with the smallest Excitation on

the premise of being as close as possible to the minimum energy target. It is necessary to optimize Eq. (51) to increase the sensitivity of distance to the energy target. With a correction coefficient introduced into Eq. (51), Eq. (52) is obtained and can be used to target the improved Utopian solution. The results are shown in Fig. 16. It can be seen that the improved Utopian solution is consistent with the actual optimal solution. Hence Eq. (52) can be used as an empirical formula for selecting Utopian solutions in optimizing Excitation and energy.

$$Distance_i = \sqrt{\left(\frac{Exicitation_i - 0}{Exicitation_{\max} - 0}\right)^2 + \left(\frac{Energy_i - 109,206}{Energy_{\max} - 109,206}\right)^2} \tag{51}$$

$$Distance_i = \sqrt{\left(\frac{Exicitation_i - 0}{Exicitation_{\max} - 0}\right)^2 + \left(8 \times \frac{Energy_i - 109,206}{Energy_{\max} - 109,206}\right)^2} \tag{52}$$

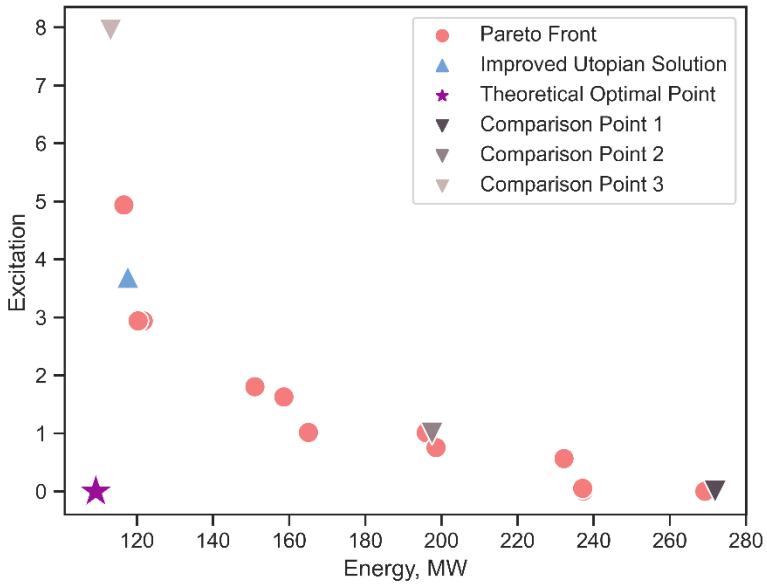

Fig. 16 Pareto front and improved Utopian solution

6.3 Comparison and Analysis of Selected Solutions

In order to highlight the superiority of the algorithm and the model, the improved Utopian solution is compared with three other solutions in Table 3. Besides, the HEN designed by the proposed method is compared with that designed by the Aspen Energy Analyzer. The specific data of the improved Utopian solution and comparison points 2 and 3 are illustrated in Appendix B. Comparison point 1 corresponds to the situation with all streams heated or cooled by the utilities and no heat exchange between streams. In this case, the Excitation of the HEN is 0, and the energy target is 271,903.77kW.

The HEN of the improved Utopian solution is shown in Fig. 17. There are four process stream heat exchangers and thirteen irrelevant subsystems. The maximum irrelevant subsystem includes three streams and two process stream heat exchangers, and the secondary maximum irrelevant subsystem consists of two streams and one process stream heat exchanger. The heating utility consumption is 117,617kW, and the Excitation is 3.67.

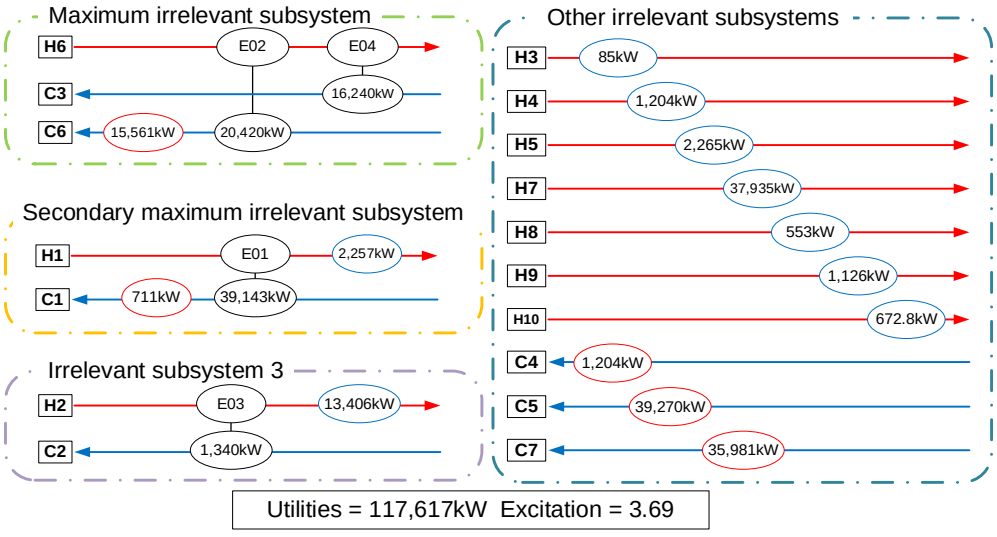

Fig. 17 HEN corresponding to the improved Utopian Solution

Table 3 Comparison of the improved Utopian solution with three other solutions

Point	Energy, kW	Excitation	Irrelevant subsystem	Process heat exchanger	Maximum irrelevant subsystem		Secondary maximum irrelevant subsystem	
					No. of streams	No. of heat exchangers	No. of streams	No. of heat exchangers
Improved Utopian solution	117,617	3.69	13	4	3	2	2	1
Comparison point 1	271,904	0.00	17	0	1	0	1	0
Comparison point 2	197,534	1.00	15	2	2	1	2	1
Comparison point 3	113,073	7.95	10	7	3	2	3	2
Aspen result	152,490	13.45	10	7	8	7	1	0

The HEN corresponding to comparison point 2 is shown in Fig. 18. Comparison point 2 contains one process stream heat exchanger and 16 irrelevant subsystems; two irrelevant subsystems consist of two streams and one process stream heat exchanger. The heating utility consumption is 197,534kW, and the Excitation is 1.

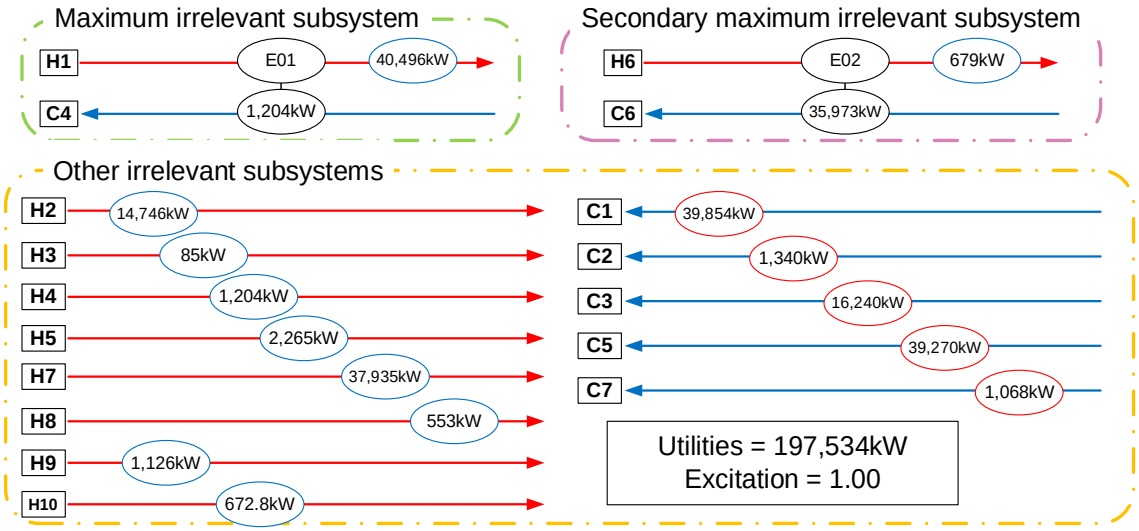

Fig. 18 HEN corresponding to the comparison point 2

As analyzed in Section 3.4, the more the process stream heat exchangers, the fewer the irrelevant subsystems; the more heat exchangers in a single irrelevant subsystem, the more complex the network and the stronger the coupling. Correspondingly, the weaker the HEN's ability to resist parameter fluctuations, the greater the Excitation. Although the Excitation of comparison point 2 is less than that of the improved Utopian solution, the utility consumed is 67.9% greater than that of the improved Utopian solution. Fig. 17 shows that the four heat exchangers of the improved Utopian solution have strong decoupling between each other, and

the Excitation is within an acceptable range. Therefore, the improved Utopian solution is better than comparison point 2.

The HEN corresponding to comparison point 3 is shown in Fig. 19. There are seven process stream heat exchangers and ten irrelevant subsystems. Two subsystems include three streams and two process stream heat exchangers. Compared with the improved Utopian solution, comparison point 3 has more process stream heat exchangers and fewer irrelevant subsystems, significantly enhancing the coupling between heat exchangers. Its heating utility consumption is 113,073kW, 2.3% less than the improved Utopian solution, while the Excitation is 7.95, 116.6% greater than that of the improved Utopian solution. Therefore, the improved Utopian solution is better than comparison point 3.

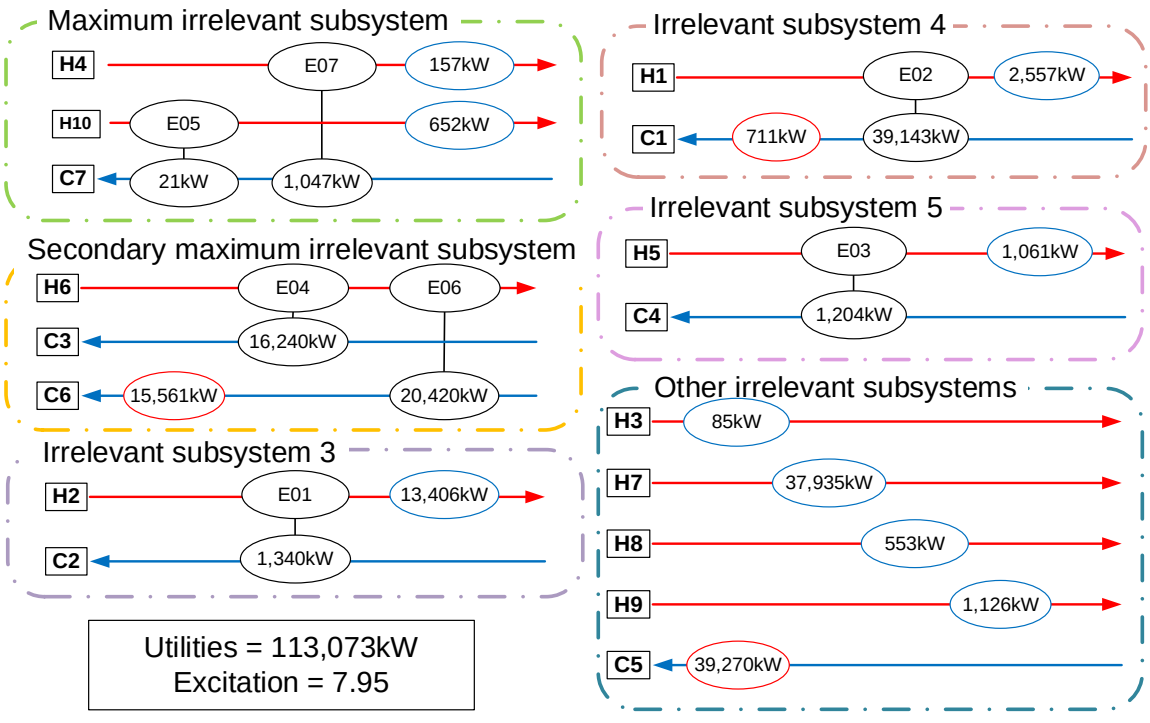

Fig. 19 HEN corresponding to the comparison point 3

The HEN designed by Aspen Energy Analyzer is shown in Fig. 20, which includes seven process stream heat exchangers and ten irrelevant subsystems. The maximum irrelevant subsystem contains eight streams and seven process stream heat exchangers. The coupling between these heat exchangers is much stronger, as the Excitation (13.45) is 264.50% greater and its energy target is 30.8% greater than the improved Utopian solution. Therefore, the HEN designed by the Aspen Energy Analyzer is inferior to the improved Utopian solution.

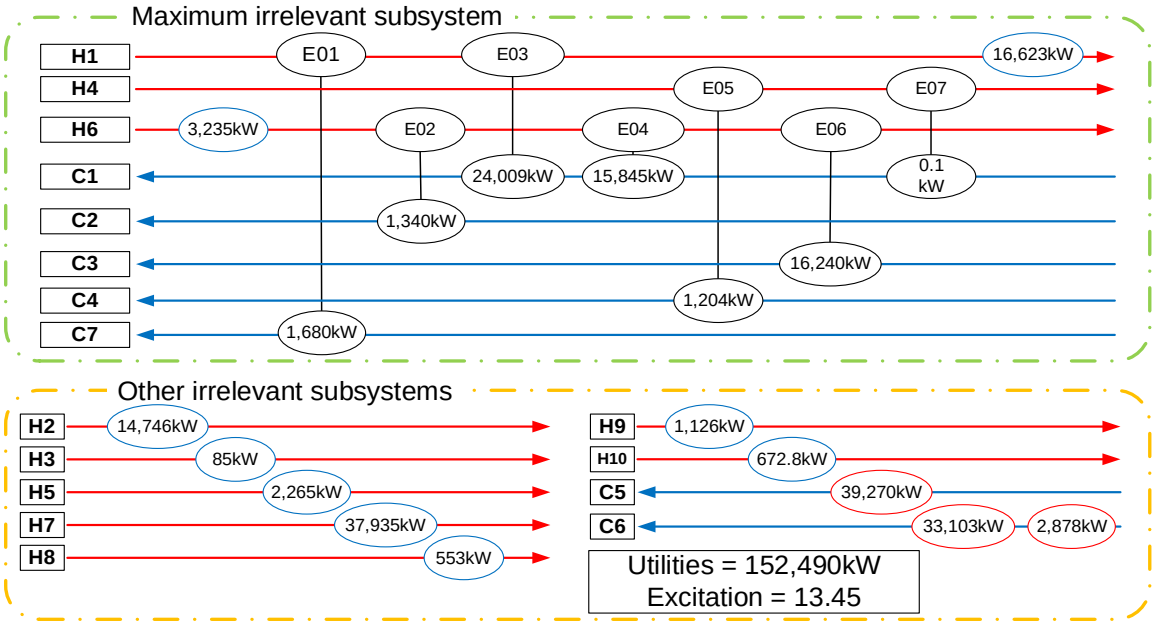

Fig. 20 The HEN Designed by Aspen Energy Analyzer

6.4 Economic Analysis

In order to verify the superiority of the improved Utopian solution further, the economic performance of the improved Utopian solution and comparison point 3 are compared.

The total cost of the HEN, the annualized investment cost, and the annual

operating cost are calculated in Eqs. (53)-(55), respectively.

$$COST_{total} = \sum_{i=1}^{n} COST_{investment,i} + \sum_{j=1}^{m} COST_{utility,j} \tag{53}$$

$$COST_{investment,i} = \frac{COST_{fixed} + \alpha area_i^{\beta}}{Year} \tag{54}$$

$$COST_{utility,j} = Hour \times \gamma QU_j \tag{55}$$

Where *COST* denotes the annualized cost, $\$\cdot y^{-1}$; *n* is the number of heat exchangers; *m* is the number of utility heat exchangers; $COST_{fixed}$ stands for the fixed investment cost of the heat exchanger and is taken as 90,400 $ (Sreepathi and Rangaiah, 2014); *area* is the heat transfer area, m^2; α and β are constants and taken as 1,127 and 0.998; *Year* is the depreciation years of heat exchanger, y; *Hour* is the annual operating time of the heat exchanger, $h\cdot y^{-1}$; *QU* is the heat load of the utility heat exchanger, kW, γ is the utility cost coefficient, $\$\cdot kJ^{-1}$, and can be calculated according to Eq. (56).

$$\gamma = \frac{CM}{CpM \times \Delta T} \tag{56}$$

Where *CM* is the media costs of utilities, $\$\cdot kg^{-1}$; ΔT is the temperature difference between the inlet and outlet medium, °C; *CpM* is the heat capacity or latent heat of the medium, $kJ\cdot°C^{-1}\cdot kg^{-1}$。

According to Sreepathi and Rangaiah (2014), the total heat transfer coefficient of the heat exchanger is set and shown in Table 4. The depreciation period is ten years, and the annual operating time is 8,000 $h\cdot y^{-1}$. The parameters related to the

utilities are shown in Table 5. The detailed data for the improved Utopian solution and comparison point 3 are shown in Appendix C.

Table 4 Total heat transfer coefficient

Process stream heat exchanger	Cooler	Heater
0.5 kW·°C $^{-1}$·m^{-2}	0.714 kW·°C $^{-1}$·m^{-2}	0.667 kW·°C $^{-1}$·m^{-2}

Table 5 Utility parameters

Utility	Cost, \$·kg^{-1}	Heat capacity, kJ·°C $^{-1}$·kg^{-1}	Difference between inlet and outlet temperatures, ℃
20℃ cooling water	2.38×10^{-5}	4.183	10
2MPa steam	1.31×10^{-2}	2,796.4	1

Based on the economic analysis, the annualized cost of the improved Utopian solution is 12.1576 million \$·y^{-1}, while that of comparison point 3 is 12.2518 million \$·y^{-1}. Although comparison point 3 requires less energy, its economic performance is inferior to the improved Utopian solution. Selecting a Utopian solution based on Eq. (52) is effective and reasonable. With the energy and Excitation targets taken into account, the proposed method can obtain a solution with a lower total cost.

7. Conclusions

A novel method is proposed to design HEN with high resistance to parameter fluctuations and evaluate the practical HEN from a decoupling perspective. Based on the Digraph, Adjacency matrix, Incidence matrix, Reachability matrix, and

Laplacian matrix, the HEN's topology structure can be comprehensively illustrated; the HEN's fluctuation transmission mechanism and path can be identified. The Excitation can indicate the HEN's decoupling degree; the relationship between the HEN and the degree of disturbance can be identified by transforming the Excitation into a graph theory problem. The multi-objective optimization mathematical model with Excitation and energy consumption as the objectives can be used to optimize the HEN and target the one with strong resistance to fluctuations. Combined NSGA-II and DFS algorithms can solve this model efficiently; the proposed strategies can enhance the solving efficiency and improve the solutions' quality.

A case study of a coal-to-methanol plant shows that the proposed method and algorithm can effectively design HENs with strong resistance to uncertain parameters under the premise of an insignificant increase in utility consumption. As for a practical HEN, it can be used to evaluate the overall impact of parameter fluctuations. In addition, the proposed correlation between graph theory and HEN is also instructive for analyzing the parameter fluctuations between different units, which provides technical support for the digital twin of the chemical process. Besides, machine learning driven combinatorial optimization is tightly related to graphs (Bengio et al., 2021; Dai et al., 2017), and transforming HEN into graph problems also lay a solid theoretical foundation for machine learning driven HEN optimization.

In the proposed method, only the isothermal mixing is considered, and stream splitting is ignored. The non-isothermal mixing and the stream splitting cannot be directly applied, and the corresponding improvement should be considered in the

future. Besides, the model can be extended with the reaction and separation units considered. Although the topological structure between different units and the HEN is generally straightforward, sensitivity analysis is often tricky due to the complexity of reaction and separation systems. The hybrid modeling method will be employed to simplify the problem so as to realize the optimization of the whole system.

Acknowledgements

Financial support provided by the National Natural Science Foundation of China (22078259) and the Department of Science and Technology of Inner Mongolia (CN) (2023YFHH0108) are gratefully acknowledged.

Nomenclature

Adjacency	Adjacency matrix of directed graph
Adjacency'	Adjacency matrix of undirected graph
$Adjacency^{\top}$	Transpose of adjacency matrix
Area	Heat transfer area, m^2
area	Heat transfer area, m^2
A, B	Any real number
CM	Medium cost of utilities, $\$\cdot kg^{-1}$
$COST_{fixed}$	Annualized fixed cost of the heat exchanger, $\$\cdot y^{-1}$
$COST_{investment}$	Annualized investment cost of the heat exchanger, $\$\cdot y^{-1}$

$COST_{total}$	Annualized total cost, $\$\cdot y^{-1}$
$COST_{utility}$	Annualized utility consumption cost, $\$\cdot y^{-1}$
Cp, CP	Heat capacity of streams, $kW\cdot h\cdot kg^{-1}\cdot{}^{\circ}C^{-1}$
CpM	Heat capacity or latent heat of the medium, $kJ\cdot℃^{-1}\cdot kg^{-1}$
Crowding	Crowding degree
d	Decision variables
Degree	Degree matrix of undirected graph
Distance	Distance from actual solution to theoretical optimal solution
$d^{(-)}$	In-degree of the node
$d^{(+)}$	Out-degree of the node
E	Edge set of directed graph
e	Edge of directed graph
Energy	Energy objective, kW
Eq	Set of equations of all heat transfer units
$Eq_{balance}$	Heat balance equation
$Eq_{transfer}$	Heat transfer equation
Excitation	Excitation objective
F	Flow rate, $kg\cdot h^{-1}$
G	Directed graph of heat exchanger network
Hour	Annual operating time of the heat exchanger, $h\cdot y^{-1}$
Incidence	Incidence matrix of directed graph

K	Total heat transfer coefficient, $kW \cdot m^{-2} \cdot ^{\circ}C^{-1}$
Laplacian	Laplacian matrix of undirected graph
LMTD	Logarithmic mean heat exchange temperature difference, ℃
N_C	Set of cold streams
N_H	Set of hot streams
N_S	Set of stages
n, m, i	Dimensions
obj	Objectives of multi-objective optimization model
P	number of the streams
pop	Entire population
Prob	Selection probability
Q	Heat exchange load, kW
QU	Heat load of the utility heat exchanger, kW
R	Nested sequence of all fluctuation transmission paths
r	Sequence of one fluctuation transmission path
rank	Solution set with the same dominance level
Reachability	Reachability matrix of directed graph
s	State variables
$\mathbf{SC}_{\mathbf{D}}^{\mathbf{S}}$	First-order sensitivity coefficient matrix of the state variable vector relative to the decision variable vector

$Sensitivity_d^s$	First-order sensitivity of the state variable relative to the decision variable
S, D	State variable vector and decision variable vector
s^*, d^*	Stable value of the variable
T	Temperature of streams, °C
t	Temperature of stages, °C
V	Node set of directed graph
v	Node of directed graph
W	Fluctuation interval of stream's inlet parameter
x	General solution of equation $Laplacian \bullet x = 0$
$Year$	Depreciation years of heat exchanger, y
Z	Binary (0-1) variables representing the existence of heat exchangers
α_1, α_2	Solution vectors of the fundamental system
γ	Utility cost coefficient, \$·kJ^{-1}
Δs, Δd	Magnitude of variable change
ΔT	Temperature difference between the inlet and outlet medium, °C
Δt_{min}	Minimum heat exchange temperature difference, °C
Subscripts	
C	Cold streams
CU	Cooling utilities

H	Hot streams
HU	Heating utilities
in	Inlet
max	Maximum
min	Minimum
out	Outlet
S	Stages
Superscripts	
in	Inlet
out	Outlet
Abbreviation	
DFS	Depth-First Search
Digraph	Directed graph
HEN	Heat exchanger network
MILP	Mixed integer linear programming
MINLP	Mixed integer nonlinear programming
No.	Number
NSGA-II	Non-dominated Sorting Genetic Algorithm II

Appendix A

Table A. 1 The serial number of nodes

Nodes	Serial number	Nodes	Serial number
v1	H1IN	v10	C3OUT
v2	H1OUT	v11	CE1
v3	H2IN	v12	CE2
v4	H2OUT	v13	HE1
v5	C1IN	v14	HE2
v6	C1OUT	v15	E1
v7	C2IN	v16	E2
v8	C2OUT	v17	E3
v9	C3IN	v18	E4

Table A. 2 Edges set and streams

Edges	Streams	Edges	Streams
e_1	H1IN→E1	e_{10}	E4→E3
e_2	E1→E3	e_{11}	E3→E2
e_3	E3→CE1	e_{12}	E2→C1OUT
e_4	CE1→H1OUT	e_{13}	C2IN→E1
e_5	H2IN→E2	e_{14}	E1→HE1
e_6	E2→E4	e_{15}	HE1→C2OUT
e_7	E4→CE2	e_{16}	C3IN→HE2
e_8	CE2→H2OUT	e_{17}	HE2→C3OUT
e_9	C1IN→E4		

Table A. 3 Pseudo-code of targeting the reachable matrix by the multiplication algorithm

Input：***Adjacency Matrix***(***Adj***)

Output：***Accessibility Matrix***(***Acc***)

1 ***S*** = ***Adj*** + ***I*** //***S*** is self-multiplication matrix，***I*** is identity matrix.

2 ***While (M*** is different before and after iteration.***):***

3 ***If(*** first iteration***)：***

4 M = S⊙S //⊙ represents Boolean operation.

5 ***Else：***

6 M = M⊙S

7 Acc = M - I

Appendix B

Table B. 1 Details of the Utopian Solution

Heat exchangers	Streams	Inlet temperature , °C	Outlet temperature , °C	Heat capacity flow rate , kW▪°C $^{-1}$	Heat flux, kW	Utility consumption, kW
E01	H1	242.00	43.00	196.70	39,143.30	117,617.15
	C1	43.00	205.06	241.54		
E02	H6	117.40	114.73	7,637.50	20,420.00	
	C6	109.20	109.26	359,810.00		
E03	H2	72.00	70.64	983.07	1,340.01	
	C2	40.00	61.00	63.81		
E04	H6	114.73	112.60	7,637.50	16,240.00	
	C3	73.00	73.80	20,300.00		
EH1	C1	205.06	208.00	241.54	710.80	
EH2	C4	74.30	89.00	81.90	1,203.93	
EH3	C5	123.00	126.00	13,090.00	39,270.00	
EH4	C6	109.26	109.30	359,810.00	15,561.00	
EH5	C7	105.00	105.10	10,680.00	1,068.00	
EC1	H1	43.00	30.00	196.70	2,557.10	
EC2	H2	70.64	57.00	983.07	13,406.04	
EC3	H3	57.00	54.00	28.33	84.99	
EC4	H4	125.00	102.00	52.35	1,204.05	
EC5	H5	112.60	44.00	33.01	2,264.49	
EC6	H7	68.00	53.00	2,529.00	37,935.00	
EC7	H8	51.00	31.00	27.65	553.00	
EC8	H9	69.00	49.00	56.30	1,126.00	
EC9	H10	109.00	40.00	9.75	672.75	

Table B. 2 Details of the comparison point 2

Heat exchangers	Streams	Inlet temperature, °C	Outlet temperature, °C	Heat capacity flow rate, kW▪°C $^{-1}$	Heat flux, kW	Utility consumption, kW
E01	H1	242.00	236.57	196.70	1,068.00	269,767.77
	C7	105.00	105.10	10,680.00		
EC1	H1	236.57	30.00	196.70	40,632.3	
EC2	H2	72.00	57.00	983.07	14,746.0	
EC3	H3	57.00	54.00	28.33	84.99	
EC4	H4	125.00	102.00	52.35	1,204.05	
EC5	H5	112.60	44.00	33.01	2,264.49	
EC6	H6	117.40	112.60	7,637.50	36,660.0	
EC7	H7	68.00	53.00	2,529.00	37,935.0	
EC8	H8	51.00	31.00	27.65	553.00	
EC9	H9	69.00	49.00	56.30	1,126.00	
EC10	H10	109.00	40.00	9.75	672.75	
EH1	C1	43.00	208.00	241.54	39,854.1	
EH2	C2	40.00	61.00	63.81	1,340.01	
EH3	C3	73.00	73.80	20,300.00	16,240.0	
EH4	C4	74.30	89.00	81.90	1,203.93	
EH5	C5	123.00	126.00	13,090.00	39,270.0	
EH6	C6	109.20	109.30	359,810.00	35,981.0	

Table B. 3 Details of the comparison point 3

Heat exchangers	Streams	Inlet temperature, °C	Outlet temperature, °C	Heat-capacity flow rate , kW▪°C $^{-1}$	Heat flux, kW	Utility consumption, kW
E01	H1	242.00	43.00	196.70	39,143.30	112,594.65
	C1	43.00	205.06	10,680.00		
E02	H6	117.40	115.60	7,637.50	13,758.75	
	C3	73.12	73.80	20,300.00		
E03	H4	125.00	102.00	52.35	1,204.05	
	C3	73.06	73.12	20,300.00		
E04	H5	112.60	73.00	33.01	1,307.20	
	C3	73.00	73.06	20,300.00		
E05	H6	117.40	115.60	7,637.50	21,727.32	
	C6	109.20	109.26	35,9810.00		
E06	H2	72.00	70.64	983.07	1,340.01	
	C2	40.00	61.00	63.81		
E07	H6	115.60	112.76	7,637.50	1,203.93	
	C4	74.30	89.00	81.90		
EC1	H1	43.00	30.00	196.70	2,257.10	
EC2	H2	70.64	57.00	983.07	13,406.04	
EC3	H3	57.00	54.00	28.33	84.99	
EC4	H5	73.00	44.00	33.01	957.29	
EC5	H7	68.00	53.00	2529.00	37,935.00	
EC6	H8	51.00	31.00	27.65	553.00	
EC7	H9	69.00	49.00	56.30	1,126.00	
EC8	H10	109.00	40.00	9.75	672.75	
EH1	C1	208.00	205.06	241.54	710.80	
EH2	C5	123.00	126.00	13,090.00	39,270.0	
EH3	C6	109.26	109.30	359,810.00	14,253.68	
EH4	C7	105.00	105.10	10,680.00	1,068.00	

Appendix C

Table C. 1 Details of Utopian Solution Cost

Heat exchangers	Heat flux, kW	Heat area, m^{-2}	Investment cost, 10^3 $	Utility cost, 10^3 $
E01	39,143.30	17,408.26	19,330.08	
E02	20,420.00	6,040.89	6,780.96	
E03	1,340.01	139.72	246.31	
E04	16,240.00	806.57	987.31	
EH1	710.80	370.96	503.55	
EH2	1,203.93	14.13	106.24	
EH3	39,270.00	692.60	860.82	932.77
EH4	15,561.00	232.76	349.88	
EH5	1,068.00	15.33	107.58	
EC1	2,557.10	311.68	437.66	
EC2	13,406.04	483.31	628.40	
EC3	84.99	3.91	94.80	
EC4	1,204.05	19.08	111.77	
EC5	2,264.49	66.83	165.08	7,938.16
EC6	37,935.00	1,496.67	1,752.66	
EC7	553.00	49.92	146.22	
EC8	1,126.00	46.65	142.57	
EC9	672.75	21.92	114.95	
Sum of individual annualized, million $\cdot y^{-1}$			3.2867	8.8709
Total annualized, million $\cdot y^{-1}$			12.1576	

Table C. 2Details of Comparison Point 3 Cost

Heat exchangers	Heat flux, kW	Heat area, m^{-2}	Investment cost, 10^3 $	Utility cost, $10^3$$
E01	1,340.01	139.72	246.31	
E02	39,143.30	17,408.26	19,330.08	
E03	1,203.93	282.33	405.02	
E04	16,240.00	756.34	931.57	
E05	21.00	15.60	107.89	
E06	20,420.00	8,888.08	9,926.76	
E07	1,047.00	799.27	979.22	
EH1	710.80	370.96	503.55	
EH2	39,270.00	692.60	860.82	896.11
EH3	15,561.00	232.76	349.88	
EC1	2,557.10	311.68	437.66	
EC2	13,406.04	483.31	628.40	
EC3	84.99	3.91	94.80	
EC4	157.05	2.80	93.55	
EC5	1,060.56	43.79	139.38	7,636.59
EC6	37,935.00	1,496.67	1,752.66	
EC7	553.00	49.92	146.22	
EC8	1,126.00	46.65	142.57	
EC9	651.75	21.59	114.58	
Sum of individual annualized, million $·$y^{-1}$			3.7191	8.5327
Total annualized, million $·$y^{-1}$			12.2518	

Reference

Aguilera, N., Nasini, G., 1995. Flexibility test for heat exchanger networks with uncertain flowrates. Computers & Chemical Engineering 19, 1007–1017. https://doi.org/10.1016/0098-1354(95)99934-B

Aguitoni, M.C., Pavão, L.V., Siqueira, P.H., Jiménez, L., Ravagnani, M.A. da S.S., 2018. Heat exchanger network synthesis using genetic algorithm and differential evolution.

Computers & Chemical Engineering 117, 82–96. https://doi.org/10.1016/j.compchemeng.2018.06.005

Bengio, Y., Lodi, A., Prouvost, A., 2021. Machine learning for combinatorial optimization: A methodological tour d'horizon. European Journal of Operational Research 290, 405–421. https://doi.org/10.1016/j.ejor.2020.07.063

Cardoso-Fernández, V., Bassam, A., May Tzuc, O., Barrera Ch., M.A., Chan-González, J. de J., Escalante Soberanis, M.A., Velázquez-Limón, N., Ricalde, L.J., 2023. Global sensitivity analysis of a generator-absorber heat exchange (GAX) system's thermal performance with a hybrid energy source: An approach using artificial intelligence models. Applied Thermal Engineering 218, 119363. https://doi.org/10.1016/j.applthermaleng.2022.119363

Dai, H., Khalil, E.B., Zhang, Y., Dilkina, B., Song, L., 2017. Learning combinatorial optimization algorithms over graphs. Advances in Neural Information Processing Systems 30, 6349–6359. https://doi.org/10.48550/arXiv.1704.01665

Deb, K., Pratap, A., Agarwal, S., Meyarivan, T., 2002. A fast and elitist multiobjective genetic algorithm: NSGA-II. IEEE Transactions on Evolutionary Computation 6, 182–197. https://doi.org/10.1109/4235.996017

Deo, N., 1975. Graph theory with applications to engineering and computer science. Networks 5, 299–300. https://doi.org/10.1002/net.1975.5.3.299

Floudas, C.A., Ciric, A.R., Grossmann, I.E., 1986. Automatic synthesis of optimum heat exchanger network configurations. AIChE Journal 32, 276–290. https://doi.org/10.1002/aic.690320215

Gu, K., Vassiliadis, V.S., 2014. Limitations in using Euler's formula in the design of heat exchanger networks with Pinch Technology. Computers & Chemical Engineering 68, 123–127. https://doi.org/10.1016/j.compchemeng.2014.05.015

Hafizan, A.M., Klemeš, J.J., Alwi, S.R.W., Manan, Z.A., Hamid, M.K.A., 2019. Temperature disturbance management in a heat exchanger network for maximum energy recovery considering economic analysis. Energies 12, 594. https://doi.org/10.3390/en12040594

Huang, Y., Zhuang, Y., Xing, Y., Liu, L., Du, J., 2023. Multi-objective optimization for work-integrated heat exchange network coupled with interstage multiple utilities. Energy 273, 127240. https://doi.org/10.1016/j.energy.2023.127240

Jiang, N., Shelley, J.D., Doyle, S., Smith, R., 2014. Heat exchanger network retrofit with a fixed network structure. Applied Energy 127, 25–33. https://doi.org/10.1016/j.apenergy.2014.04.028

Kang, L., Liu, Y., 2018a. A Three-step method to improve the flexibility of multiperiod heat exchanger networks. Process Integration and Optimization for Sustainability 2, 169–181. https://doi.org/10.1007/s41660-018-0034-5

Kang, L., Liu, Y., 2018b. Design of flexible multiperiod heat exchanger networks with debottlenecking in subperiods. Chemical Engineering Science 185, 116–126. https://doi.org/10.1016/j.ces.2018.04.017

Kang, L., Tang, W., Liu, Y., Daoutidis, P., 2016. Control configuration synthesis using agglomerative hierarchical clustering: A graph-theoretic approach. Journal of Process Control 46, 43–54. https://doi.org/10.1016/j.jprocont.2016.07.009

Kemp, I.C., 2007. Key concepts of pinch analysis, in: Kemp, I.C. (Ed.), Pinch Analysis and Process Integration (Second Edition). Butterworth-Heinemann, Oxford, pp. 15–40. https://doi.org/10.1016/B978-075068260-2.50007-9

Li, J., Du, J., Zhao, Z., Yao, P., 2015. Efficient method for flexibility analysis of large-scale nonconvex heat exchanger networks. Industrial and Engineering Chemistry Research 54, 10757–10767. https://doi.org/10.1021/acs.iecr.5b00237

Li, J., Du, J., Zhao, Z., Yao, P., 2014. Structure and area optimization of flexible heat exchanger networks. Industrial and Engineering Chemistry Research 53, 11779–11793. https://doi.org/10.1021/ie501278c

Li, J., Xiao, X., Boukouvala, F., Floudas, C.A., Zhao, B., Du, G., Su, X., Liu, H., 2016. Data-driven mathematical modeling and global optimization framework for entire petrochemical planning operations. AIChE Journal 62, 3020–3040. https://doi.org/10.1002/aic.15220

Linnhoff, B., Hindmarsh, E., 1983. The pinch design method for heat exchanger networks. Chemical Engineering Science 38, 745–763. https://doi.org/10.1016/0009-2509(83)80185-7

Linnhoff, B., Kotjabasakis, E., 1986. Downstream paths for operable process design. Chemical Engineering Progress 82, 23–28.

Miranda, C.B., Costa, C.B.B., Caballero, J.A., Ravagnani, M.A.S.S., 2016. Heat exchanger network optimization for multiple period operations. Industrial and Engineering Chemistry Research 55, 10301–10315. https://doi.org/10.1021/acs.iecr.6b01117

Mohanan, K., Jogwar, S.S., 2022. Optimal operation of heat exchanger networks through energy flow redistribution. AIChE Journal 68, e17716. https://doi.org/10.1002/aic.17716

Nie, Y., Avraamidou, S., Xiao, X., Pistikopoulos, E.N., Li, J., 2019. Two-stage land use optimization for a Food-Energy-Water Nexus system: A case study in Texas Edwards region. Computer Aided Chemical Engineering 47, 205–210. https://doi.org/10.1016/B978-0-12-818597-1.50033-3

Nie, Y., Avraamidou, S., Xiao, X., Pistikopoulos, E.N., Li, J., Zeng, Y., Song, F., Yu, J., Zhu, M., 2018. A Food-Energy-Water Nexus approach for land use optimization. Science of the Total Environment 659, 7–19. https://doi.org/10.1016/j.scitotenv.2018.12.242

Papoulias, S.A., Grossmann, I.E., 1983. A structural optimization approach in process synthesis—II: Heat recovery networks. Computers & Chemical Engineering 7, 707–721. https://doi.org/10.1016/0098-1354(83)85023-6

Ratnam, R., Patwardhan, V.S., 1991. Sensitivity analysis for heat exchanger networks. Chemical Engineering Science 46, 451–458. https://doi.org/10.1016/0009-2509(91)80006-K

Ryu, J., Kong, L., Pastore de Lima, A.E., Maravelias, C.T., 2020. A generalized superstructure-based framework for process synthesis. Computers & Chemical Engineering 133, 106653. https://doi.org/10.1016/j.compchemeng.2019.106653

Shivakumar, K., Narasimhan, S., 2002. A robust and efficient NLP formulation using graph theoretic principles for synthesis of heat exchanger networks. Computers & Chemical Engineering 26, 1517–1532. https://doi.org/10.1016/S0098-1354(02)00089-3

Sreepathi, B.K., Rangaiah, G.P., 2014. Improved heat exchanger network retrofitting using exchanger reassignment strategies and multi-objective optimization. Energy 67, 584–594. https://doi.org/10.1016/j.energy.2014.01.088

Tarjan, R., 1971. Depth-first search and linear graph algorithms, in: 12th Annual Symposium on Switching and Automata Theory (Swat 1971). IEEE. pp. 114–121. https://doi.org/10.1109/SWAT.1971.10

Tian, Y., Li, S., 2023. Cost allocation evaluation of a multi-plant flexible heat exchanger network design based on fuzzy game. Computers & Chemical Engineering 175, 108262. https://doi.org/10.1016/j.compchemeng.2023.108262

Wang, K., Qian, Y., Huang, Q., Yuan, Y., Yao, P., 1999. New model and new algorithm for optimal synthesis of large scale heat exchanger networks without stream splitting. Computers & Chemical Engineering 23, S149–S152. https://doi.org/10.1016/S0098-1354(99)80037-4

Warshall, S., 1962. A Theorem on Boolean matrices. Journal of the ACM (JACM) 9, 11–12. https://doi.org/10.1145/321105.321107

Xu, Y., Cui, G., 2023. Intelligent search strategy applied in heat exchanger network synthesis. Energy Reports 9, 11–27. https://doi.org/10.1016/j.egyr.2023.02.062

Xu, Y., Zhang, L., Cui, G., Yang, Q., 2023. A heuristic approach to design a cost-effective and low-CO2 emission synthesis in a heat exchanger network with crude oil distillation units. Energy 271, 126972. https://doi.org/10.1016/j.energy.2023.126972

Yang, Y.H., Gong, J.P., Huang, Y.L., 1996. A simplified system model for rapid evaluation of disturbance propagation through a heat exchanger network. Industrial and Engineering Chemistry Research 35, 4550-4558. https://doi.org/10.1021/ie960321c

Ye, Y., Li, J., Li, Z., Tang, Q., Xiao, X., Floudas, C.A., 2014. Robust optimization and stochastic programming approaches for medium-term production scheduling of a large-scale steelmaking continuous casting process under demand uncertainty. Computers & Chemical Engineering 66, 165–185. https://doi.org/10.1016/j.compchemeng.2014.02.028

Yee, T.F., Grossmann, I.E., Kravanja, Z., 1990. Simultaneous optimization models for heat integration—I. Area and energy targeting and modeling of multi-stream exchangers. Computers & Chemical Engineering 14, 1151–1164. https://doi.org/10.1016/0098-1354(90)85009-Y

Zeng, Y., Xiao, X., Li, J., Sun, L., Floudas, C.A., Li, H., 2018. A novel multi-period mixed-integer linear optimization model for optimal distribution of byproduct gases, steam and power in an iron and steel plant. Energy 143, 881–899. https://doi.org/10.1016/j.energy.2017.10.122

Zhang, D., Lv, D., Yin, C., Liu, G., 2020. Combined pinch and mathematical programming method for coupling integration of reactor and threshold heat exchanger network. Energy 205, 118070. https://doi.org/10.1016/j.energy.2020.118070

Zhao, L., Liu, G., 2023. Bottleneck-identification methodology and debottlenecking strategy for heat exchanger network with disturbance. Chemical Engineering Science 275, 118727. https://doi.org/10.1016/j.ces.2023.118727

Zhao, L., Liu, G., 2022. Dynamic coupling of reactor and heat exchanger network considering catalyst deactivation. Energy 260, 125161. https://doi.org/10.1016/j.energy.2022.125161

Zhu, J., Han, Z., Rao, M., Chuang, K., 1996. Identification of heat load loops and downstream paths in heat exchanger networks. Canadian Journal of Chemical Engineering 74, 876–882. https://doi.org/10.1002/cjce.5450740609

Declaration of interests

☒ The authors declare that they have no known competing financial interests or personal relationships that could have appeared to influence the work reported in this paper.

☐The authors declare the following financial interests/personal relationships which may be considered as potential competing interests:
